



Origin and Evolution of the Halo-Volcanic Complex of Dallol: Proto-Volcanism in Northern Afar (Ethiopia)

José M. López-García^{1*}, David Moreira², Karim Benzerara³, Olivier Grunewald⁴ and Purificación López-García²

¹ Instituto Geológico y Minero de España, Palma de Mallorca, Spain, ² Unité d'Ecologie, Systématique et Evolution, CNRS, AgroParisTech, Université Paris-Saclay, Orsay, France, ³ Institut de Minéralogie, de Physique des Matériaux et de Cosmochimie, CNRS, Muséum National d'Histoire Naturelle, Sorbonne Université, Paris, France, ⁴ Association Aux Origines du Monde, Paris, France

OPEN ACCESS

Edited by:

Valerio Acocella,
Roma Tre University, Italy

Reviewed by:

Joël Ruch,
Université de Genève, Switzerland
Orlando Vaselli,
University of Florence, Italy

*Correspondence:

José M. López-García
jm.lopez@igme.es

Specialty section:

This article was submitted to
Structural Geology and Tectonics,
a section of the journal
Frontiers in Earth Science

Received: 29 August 2019

Accepted: 18 December 2019

Published: 17 January 2020

Citation:

López-García JM, Moreira D, Benzerara K, Grunewald O and López-García P (2020) Origin and Evolution of the Halo-Volcanic Complex of Dallol: Proto-Volcanism in Northern Afar (Ethiopia). *Front. Earth Sci.* 7:351. doi: 10.3389/feart.2019.00351

Contextual early observations on volcano genesis are valuable but scarce. Resembling a shield volcano, the Dallol dome is a complex 40 m-high geological structure on the Danakil depression, a North-South-elongated salt plain lying 120 m below sea level in the North Afar (Ethiopia). Dallol has become a tourist destination famous for its colorful hydrothermal features and raised scientific interest due to its life-challenging polyextreme conditions. Although some general models for its genesis exist, little is known about the origin and temporal evolution of both, the dome and its geothermal activity resulting in hyperacidic and halite-oversaturated brines. In this study, we combine published information with data obtained from our three multidisciplinary field campaigns (January 2016, 2017, and 2019) to refine the geological mapping of the North Danakil and the Dallol dome. The analysis of stratigraphic, geomorphological, geochemical, and hydrogeochemical data as well as satellite, drone and infrared aerial images allows us to shed light in its complex temporal evolution. Our results suggest that the recorded history of the dome began when at least one deep magmatic basalt intrusion occurred later than 6000 years ago, forcing the uplifting of the lacustrine deposits of that age covering the west side of the dome. The interaction of the magma with the buried salt deposit resulted in a halo-volcanic activity with, likely, several melted-salt effusion events. Substrate accommodation after effusion led to the current collapsing crater on the dome top and the geothermal still-ongoing degassing. An important hydrothermal reactivation took place after a dyke intrusion event in October–November 2004. It triggered the appearance of new fractures on the dome top and the northward migration of the hydrothermal activity, as we inferred from the analysis of historical aerial images combined with high-definition visible and infrared images taken from a drone during our field campaigns. Based on our observations, we present an updated hydrogeothermal conceptual model linking deep magmatic activity with halokinetic processes and geothermal fluids to explain the origin and evolution of the Dallol halo-volcanic complex. These geothermal manifestations may potentially inform about rarely documented premises of a volcano's birth.

Keywords: Dallol dome, Danakil depression, proto-volcanism, halo-volcanism, salt volcano, hydrothermal vent, anhydrite, bischofite

INTRODUCTION

Direct observations of volcano formation including very early contextual genetic steps are extremely rare. The dome of Dallol, located in the tectonically, seismically, and volcanically active North Ethiopian Afar region may offer a suitable model for such processes. The dome of Dallol is a complex geological feature raising 40 m high over the salt plain of the Danakil depression. The complex is equidistant to the volcanic edifices of Maraho and Gada Ale located ca. 33 km to the, respectively, NNW and SSE direction along the depression, aligned with the main Holocene volcanoes punctuating the Northern Afar Rift axis (Corti et al., 2015). The Danakil depression is a N-S basin ca. 200 km long, 50–150 km wide and down to 120 m below sea level (bsl), lying at the triple junction between the Nubian, Somalian, and Arabian plates and the Danakil microplate (Hutchinson and Engels, 1972; Collet et al., 2000; Eagles et al., 2002; Tesfaye et al., 2003; Bonatti et al., 2015; Corti et al., 2015; Bastow et al., 2018; **Figure 1A**). Two noticeable escarpments limit the depression. To the west, the Northern Ethiopian Plateau, of Precambrian and Mesozoic origin, culminates at more than 2000 m of altitude. To the east, the less prominent Danakil Alps sit on a tectonic microplate, the Danakil Block, uprising 500–1000 m above sea level (Collet et al., 2000). The salt plain formed when the northern extremity of an ancient Red Sea arm was closed at the Gulf of Zula (Eritrea) due to uplift and doming preceding the Alid volcano Quaternary magma flows (Lalou et al., 1970; Bonatti et al., 1971; Mitchell et al., 1992; Corti et al., 2015). This closure possibly happened during the Pleistocene and left marine reefs at different altitudes (−30 to +90 m), marking ancient shorelines (Barberi and Varet, 1970; Bonatti et al., 1971; Hutchinson and Engels, 1972; Mitchell et al., 1992; Talbot, 2008). Subsequent seawater evaporation led to the deposition of a ~2 km thick salt sequence over several thousand years (Bonatti et al., 1971).

The dome of Dallol consists of protruding bedded-halite and anhydrite layers dipping gently outwards outlining an elliptical structure elongated in E-W direction, partially covered by overimposed geothermal deposits. A central depression of 1 km in diameter gives to the Dallol dome a crater-like appearance (Holwerda and Hutchinson, 1968; Talbot, 2008; Franzson et al., 2015). The volcano-like morphology, geothermal activity and location of the dome on the Danakil depression axis (between the Erta Ale volcanic ridge in the south and the Maraho, Alid, and Jalua volcanoes in the north) has led many authors to refer to this structure as the “Dallol volcano” (Edelmann et al., 2010; Darrah et al., 2013; Keir et al., 2013; Tadiwos, 2013; Wunderman, 2013; Corti et al., 2015). However, volcanic materials have never been found on the dome or its immediate surroundings. The Dallol dome is exclusively composed of salt deposits coming from uplifted primary halite beds controlled by the presence of a shallow magmatic chamber (Nobile et al., 2012), and derived halokinetic processes (Talbot, 2008; Warren, 2015c). An intense geothermal activity, which occasionally includes phreatic explosions and is mainly controlled by poorly understood interactions between magma, deep hydrated salts and groundwater, results in the world-renowned colorful acidic brine ponds, fumaroles, small geysers, salt deposits, and other

hydro-geothermal manifestations (Holwerda and Hutchinson, 1968; Hovland et al., 2006; Talbot, 2008; Franzson et al., 2015; Warren, 2015a; Varet, 2018). The result of such interactions is a particularly extreme environment with brines exhibiting low pH (≤ 0), high salt contents (>30%) and high temperatures (up to ~110°C) (Belilla et al., 2019), undergoing a hyper-arid climate (<200 mm/year rainfall) with the official world record of the highest annual mean temperature (34.5°C; Pedgley, 1967). Other minor geothermal-related structures are located around the Dallol dome. These include the Round Mountain to the west (3 km away from the central crater), the Black Mountain in the southwest (2 km away), the Horseshoe Mountain in the east and the Yellow Lake (Ga’et Ale) southeast (4 km away), as well as many other small bubbling springs and ponds of geothermal origin (**Figure 1B**).

Dallol has also attracted attention as a potential analog of some Mars regions (Cavalazzi et al., 2019). The brines of the geothermal field of Dallol combine unique polyextreme conditions that are limiting for life (Belilla et al., 2019). However, although some general models to explain the genesis of the dome have been proposed (Talbot, 2008; Carniel et al., 2010; Franzson et al., 2015; Warren, 2015c), a comprehensive model about the origin and temporal evolution of both, the dome and its geothermal activity resulting in hyperacidic and salt-oversaturated brines is still lacking. In this work, we combine geological mapping, petrographic characterization and satellite and aerial image analysis to constraint the spatio-temporal origin and evolution of the Dallol dome and its geothermal activity. We propose a detailed hydrogeothermal conceptual model and tentatively predict the future evolution of the dome. The geothermal activity of Dallol probably represents a proto-volcanic manifestation related to extensional faulting and magma intrusion in this rift segment. Beyond its local specificity, our study may have implications to understand the early steps of (proto)volcano formation.

GEOLOGICAL SETTING

The updated geological map (**Figure 1B**) and chronostratigraphic chart (**Figure 2**) after Brinckmann and Kürsten (1971) and the CNR-CNRS Afar Team (1973) along with the constructed geological cross section (**Figure 1C**) provide an overview of the known overall history of the Danakil depression. The Danakil comprises pre-rift deposits of the Precambrian to Paleozoic basement, discordantly covered by fluvial Jurassic sandstones of the Adigrat Formation and marine limestones of the Antalo Formation (no. 4 in **Figures 1B, 2, 3A**). After the Palaeogene rifting process, the erosion of the resulting blocks led to the deposition of the detrital Neogene-Pleistocene alluvial fans of the Danakil Formation (no. 5 in **Figures 1B, 2, 3A**) indented or covered by biogenic reefs. The Afar basalts intruded the faults during the Neogene (no. 1 in **Figures 1B, 2**) and different marine incursions during the Pleistocene developed the reef and coralgall biostrome patches of the Zariga Formation along an ancient coastline now visible at ca. the topographic zero level in Dallol

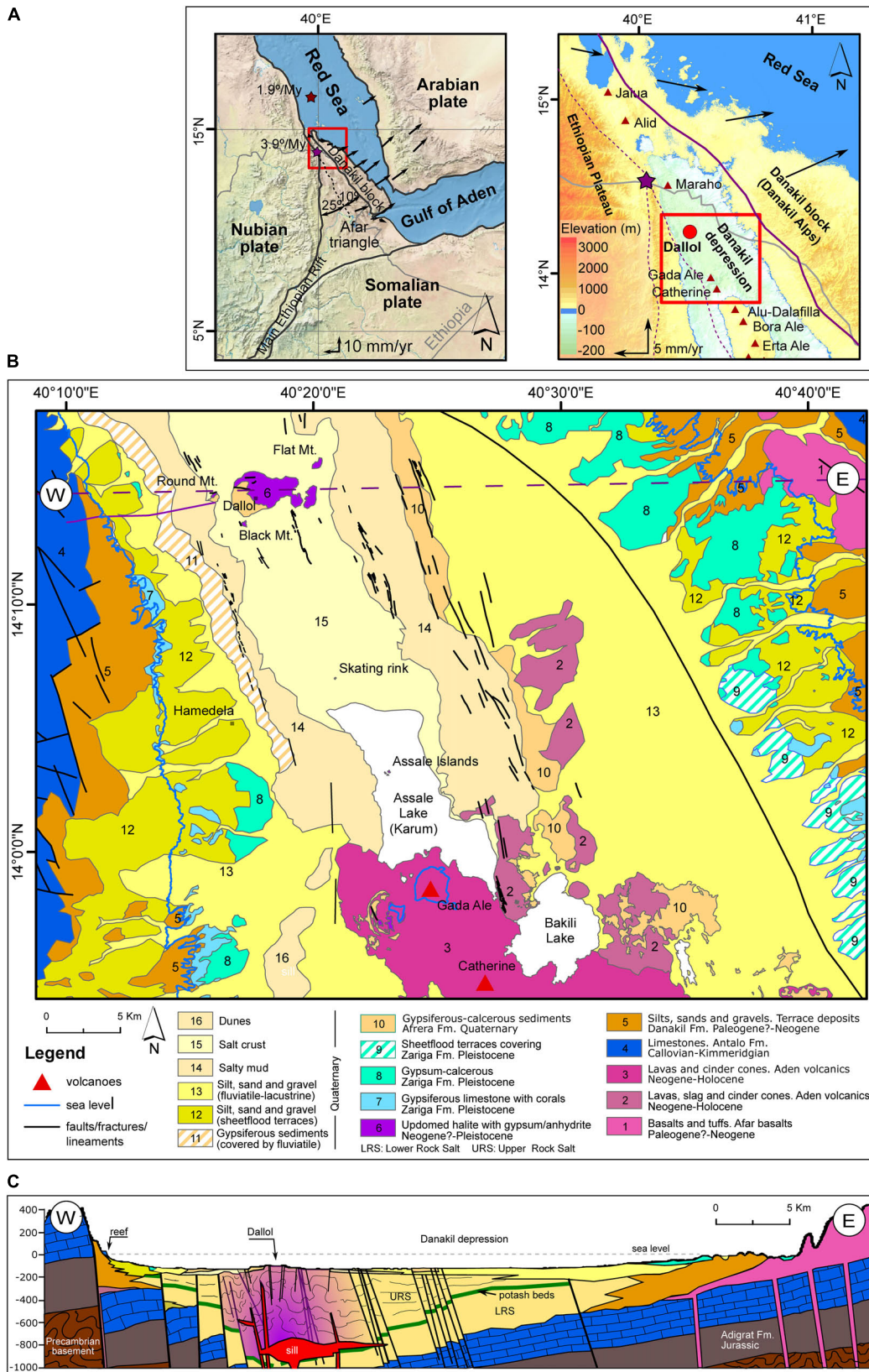


FIGURE 1 | Continued

FIGURE 1 | Location and geological map of the Dallol area. **(A)** Location of the Afar triangle between the Red Sea, Gulf of Aden, and the Main Ethiopian Rift (left). Main geographical and geological features around the studied area of Dallol in the north Afar Danakil depression, below sea level (right). Red triangles correspond to main volcanoes of the Erta Ale ridge (south of Dallol) and Alid region (north of Dallol). Arrows show backrotation of the western side of the Danakil block: 10° around Nubian-Danakil pole (red star) and 25° around a secondary pole (purple star) (Reilinger and McClusky, 2011). **(B)** Geological map [modified after Brinckmann and Kürsten (1971)]. **(C)** Cross section through the Dallol dome with the position of the most recent geological features related with the rifting process.

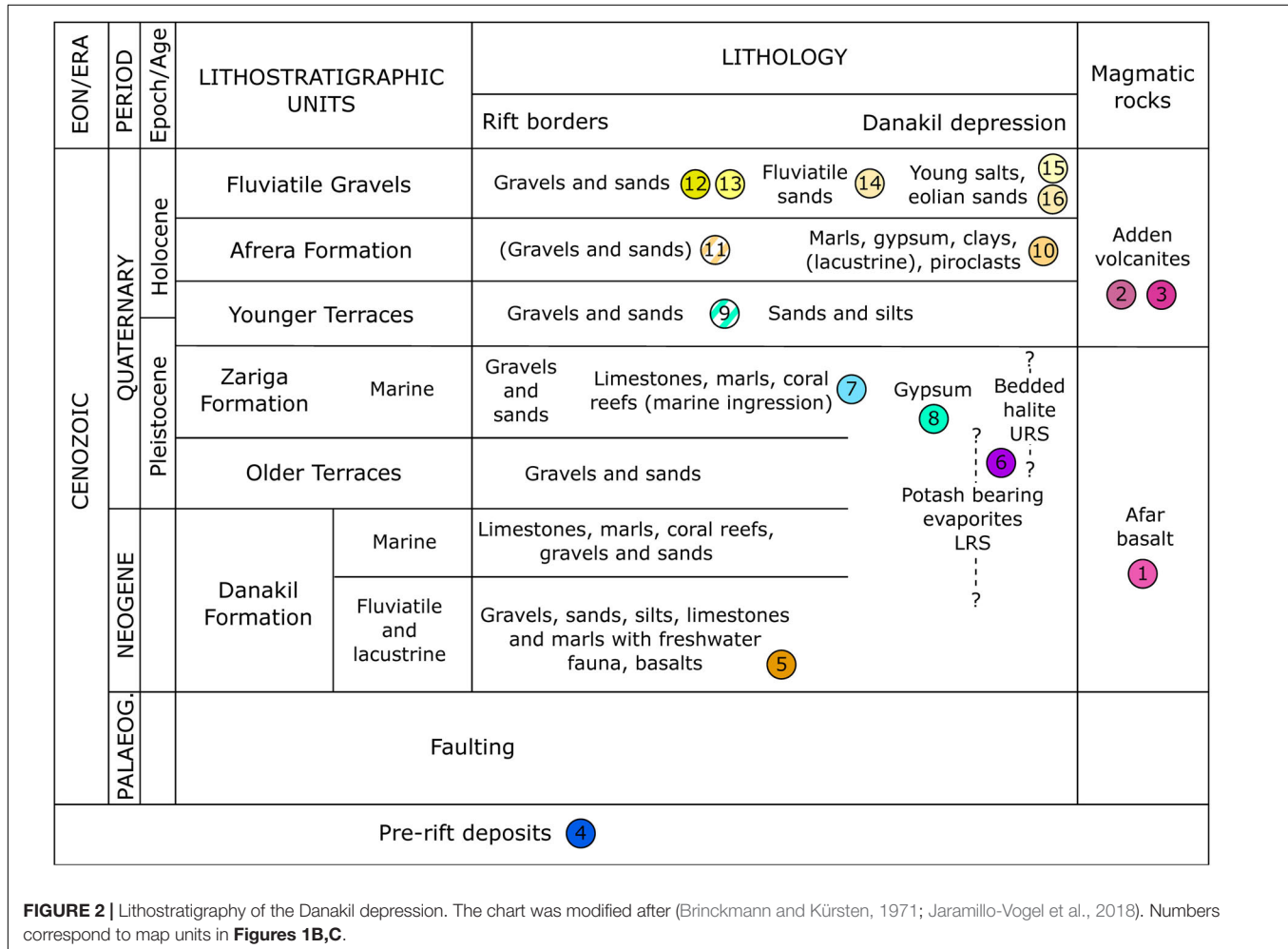


FIGURE 2 | Lithostratigraphy of the Danakil depression. The chart was modified after (Brinckmann and Kürsten, 1971; Jaramillo-Vogel et al., 2018). Numbers correspond to map units in **Figures 1B,C**.

surroundings (no. 7 in **Figures 1B, 2**). Uranium/thorium dating on corals and *Tridacna* shells showed at least two marine incursions at ca. 230 ka and 120 ka (Lalou et al., 1970; Jaramillo-Vogel et al., 2018).

The closure of the seawater passage led to the formation of a classical evaporitic drawdown facies belt from the depression margins to the center (Holwerda and Hutchinson, 1968; Warren, 2015b). The open marine reef facies transitioned to marine-seepage gypsum pavements (Hutchinson and Engels, 1970; Bastow et al., 2018) that can be seen below the reef rim (no. 8 in **Figures 1B, 2**). Drilling cores from the inner part of the depression have shown a buried sequence (ca. 1000 m thick) of halite-dominated Quaternary evaporites (Holwerda and Hutchinson, 1968; Warren, 2015a) locally covered by a thin veneer of clastic sediments. Gravimetric, magnetic and seismic reflection data suggested a total evaporitic sequence thickness

of at least 2.2 km (Behle et al., 1975). Two main thick halite sequences can be identified: the lower rock salt formation (LRS) and the upper rock salt formation (URS) (**Figure 1C**) separated by a potash unit, the Houston Formation, which has been the target of mining exploration since the beginning of the last century (Holwerda and Hutchinson, 1968). Although the age of the complete salt series is unknown, K/Ar dating at different depths in the URS suggested ages of 76 ka at 73 m depth and 88 ka at 137 m depth (Barberi et al., 1972) confirming a Pleistocene origin in agreement with the age of the last marine incursion (Jaramillo-Vogel et al., 2018) and with the ~100 ka age estimated for the onset of the last evaporative sequence (Bastow et al., 2018). The LRS extends from the Pleistocene (upper sequence part) to likely the Miocene (bottom sequence), probably being a lateral marine facies equivalent to the Danakil Formation. Likewise,

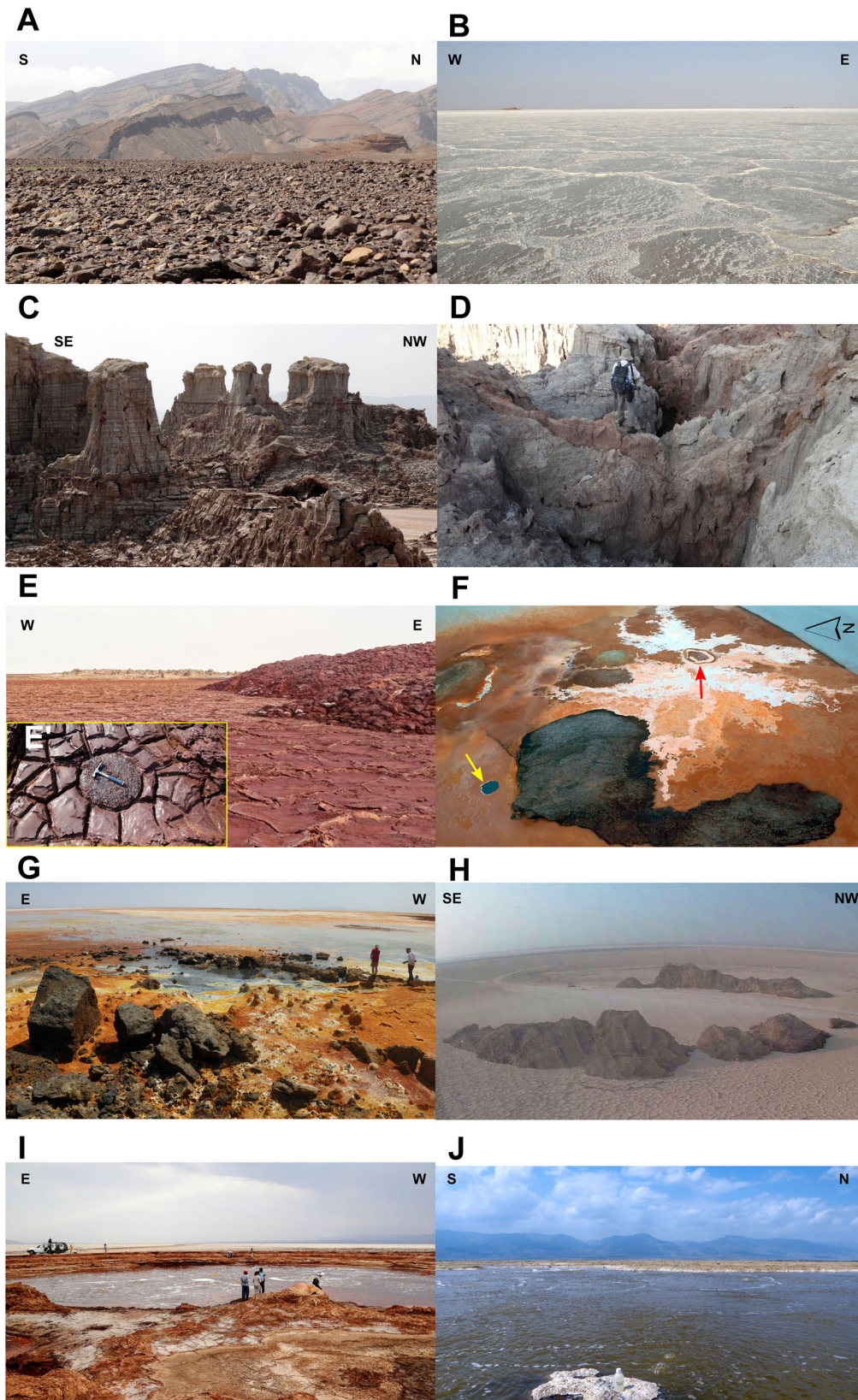


FIGURE 3 | Continued

FIGURE 3 | Geological features observed in the North Danakil depression. **(A)** Faulted and tilted blocks of the Antalo limestones and gravels of the Danakil Formation. **(B)** Salt crust of the Danakil salt plain. **(C)** Demoiselles formed by bedded halite protected from dissolution by top anhydrite layer in the Salt Canyons of western Dallol dome. **(D)** Detail of the intense karstification in the bedded halite of the Salt Canyons. **(E)** Black dome intruded in the bottom of the Dallol crater. **(E'**, detail of hexagonal joints on the Black dome). **(F)** Aerial view of the Black Mountain, with the Black Lake (yellow arrow) and bischofite flows around emission center (red arrow). **(G)** Explosive geothermal activity in the Black Mountain evidenced by the presence of big salt boulders. **(H)** Circular ring of outside dipping salts of the Skating rink. **(I)** Bubbling Yellow Lake. **(J)** Degassing lakes north to the Round Mountain. Photographs were taken during our field trips (January 2016, 2017, and 2019).

the URS might be considered a lateral equivalent of the Zariga Formation (**Figure 2**), as the last evaporitic sequence after precipitation of the Danakil depression marine-seepage-derived gypsum levels.

During the Holocene, the main reliefs continuously eroded and formed coalescent alluvial fans fringing the base of the escarpments limiting the depression (no. 11–13 in **Figures 1B, 2**). At the same time, a lacustrine system set up in the Danakil depression, as evidenced by the occurrence of white marls, marly limestones rich in diatoms, and gypsums of the Afrera Formation (no. 14 in **Figures 1B, 2**) that surrounds the Assale, Bakili and Afrera Lakes (Brinckmann and Kürsten, 1971; ERCOSPLAN, 2010). ¹⁴C-dating on *Melania* shells collected 25 km northwest of Lake Afrera gave an age of 5840 ± 205 years for this formation (Brinckmann and Kürsten, 1971). The top of the Danakil depression is capped by a non-marine salt crust (no. 15 in **Figures 1B, 2, 3B**). This several meter-thick modern salt plain comprises halite stacks, with intercalated thin mud layers (no. 14 in **Figures 1B, 2**) originated from the dissolution, evaporation and re-precipitation of previous salt bodies (Holwerda and Hutchinson, 1968) during flooding episodes and/or by the displacement of the Lake Assale to the north due to intense winds acting over the flat topography of the depression (**Figure 4**).

MATERIALS AND METHODS

Field Trips

Field data were collected during three multidisciplinary expeditions in 2016, 2017 and 2019. During the two first expeditions (16–24 January 2016; 6–15 January 2017), we explored and collected brine and solid samples (collectively, over 200 samples) from the Dallol dome hyperacidic ponds, the Salt Canyons, the Black Mountain (including the Black Lake) and the Yellow Lake areas (**Figure 1**). In 2016, we also collected water samples from Lake Assale (Lake Karum), ca. 30 km south to Dallol, on the northern side of the Erta Ale volcanic chain. In addition to geological observations, field and laboratory analyses were performed to characterize the local physicochemistry of the different local polyextreme environments, determine whether life can thrive under those conditions (Belilla et al., 2019) and study brine chemical evolution and the dynamics of mineral precipitation (Kotopoulou et al., 2019). During the third field trip (12–26 January 2019), we revisited the previously sampled areas and we extended our exploration to the Round Mountain and to different lakes around the Erta Ale volcanic range: Lake

Assale (Karum), Lake Bakili and several unnamed small lakes (**Figures 1A,B**). Their exploration was carried out with the help of a helicopter, which allowed us to land on the very small islands of Lake Assale.

Mapping and Geological Cross-Section

We updated a previous geological map of the Danakil depression (Brinckmann and Kürsten, 1971; CNR-CNRS Afar Team, 1973) through careful analysis of historical satellite images. We also carried out a detailed geological map of the Dallol dome by updating previous maps (Franzson et al., 2015) with new field data and aerial photo-interpretation from drone images taken during our three field campaigns as well as historical images obtained from Google Earth. The identification of detailed relationships among different geological units has allowed us to refine the chronostratigraphic framework needed to infer the temporal evolution of doming. We reconstructed an E-W geological cross section through the Dallol dome structure using underground information from drilling campaigns, gravimetric, and geophysical investigations published after potash exploration campaigns (Holwerda and Hutchinson, 1968; ERCOSPLAN, 2011; Franzson et al., 2015; Warren, 2015b,c,d) and structural and depth data (Nobile et al., 2012; Pagli et al., 2012; Bastow et al., 2018).

Satellite and Aerial Photographs

To identify and date the main geothermal events and the evolution of this activity in recent decades, we visualized more than one thousand freely distributed satellite images of the NASA and the US Geological Survey (USGS) Landsat program, from 1972 to 2019, as well as the Sentinel project of the Copernicus program of the European Space Agency (ESA), from 2015 to the present. A total of 98 images from Landsat 1–5 with an orbit cycle of 18 days and a ground resolution of 60 m, 323 images from Landsat 4–5, 279 images from Landsat 7 and 152 images from Landsat 8 all of them with an orbit cycle of 16 days and 30 m resolution, and 205 images from Sentinel 2 with an orbit cycle of 10 days and 10 to 60 m resolution, were taken from the Global Visualization Viewer (GloVis) courtesy of the U.S. Geological Survey¹. All images are taken from Level-1 collections with standard processing parameters detailed^{2,3} for Landsat and Sentinel, respectively. We also used six aerial images taken between 2003 and 2019 from Google Earth historical

¹<https://glovis.usgs.gov>

²<https://www.usgs.gov/land-resources/nli/landsat/landsat-collection-1>

³<https://sentinel.esa.int/web/sentinel/user-guides/sentinel-2-msi/processing-levels/level-1>

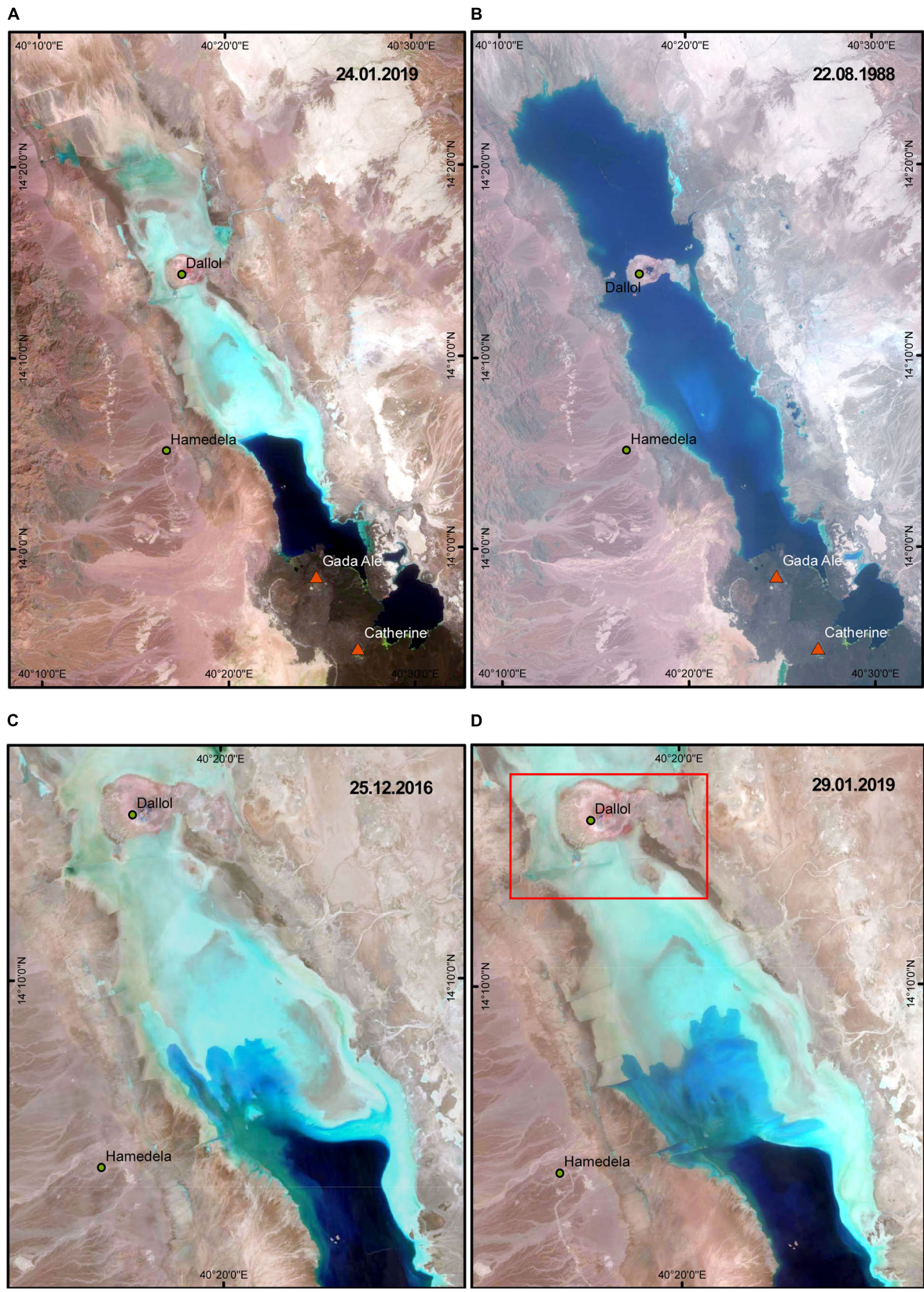


FIGURE 4 | Continued

FIGURE 4 | Satellite view of the north Danakil depression across time. Satellite images were taken during a dry period (**A**) and a humid period with the salt plain flooded (**B**) when the Dallol dome became an island. (**C,D**) Two different images showing the digitation of the Assale Lake to the north due to strong winds moving water in the flat topography of the salt plain. Red square in (**D**) corresponds to mapping area of **Figure 5**. (**A,D** Sentinel satellite images of the Galileo ESA program; **B,D** Landsat5 and Landsat8 satellite images of the NASA-USGS Landsat program).

imagery⁴. The evolution of the geothermal activity of the Dallol complex from satellite scenes can be seen in **Supplementary Video S1** along with additional close-up views from Google Earth over the Dallol crater and around the Black Mountain. For detailed mapping of the geothermal activity, we took preliminary aerial images over the active geothermal areas of Dallol, Black Mountain and Yellow Lake during the 2016 and 2017 field trips using a Phantom 2 drone equipped with a Gopro camera. For the 2019 field trip, we equipped a Phantom 4 drone with a high-resolution Gopro camera and an infrared FLIR Duo R camera and carried out carefully planned photogrammetric flights covering the geothermal active area in the summit of the Dallol dome and the Black Mountain at 110 m flight elevation with a resolution of 2 cm/pixel. In the salt canyons (western flank of the dome), flights were planned at different altitudes, at a maximum of 125 m high and 3 cm/pixel of ground resolution, to obtain a preliminary 3D composition with the software Pix 4D for future studies of the evolution of this area.

Scanning Electron Microscopy and Identification of Crystalline Phases

To differentiate mapped salt deposits, crystalline phases in representative solid samples collected at the Dallol dome and surroundings were characterized by x-ray diffraction (XRD) using X'Pert PRO Theta/Theta diffractometers (Panalytical) at the SIDI service (Universidad Autónoma de Madrid) and IMPMC (Paris). Phases were identified by comparison with the International Centre for Diffraction Data (ICDD) PDF-4+ database using the “High Score Plus” software (Malvern Panalytical⁵). In addition, to establish possible relationships between anhydrite-gypsum layers of the Dallol dome, which have an unknown chronostratigraphic position, with other surrounding gypsum levels of known chronostratigraphic position and absolute dating, selected samples were observed by scanning electron microscopy (SEM) and energy dispersive x-ray spectrometry (EDXS) analyses on morphologically identifiable structures. SEM analyses were carried using a Zeiss ultra55 field emission gun (FEG) SEM. Secondary electron (SE2) and backscattered electron (AsB) images were acquired at an accelerating voltage of 15 kV and a working distance of ~7.5 mm. Elemental maps were generated from hyperspectral images (HyperMap) by EDXS using an EDS QUANTAX detector. EDXS data were analyzed using the ESPRIT software package (Bruker).

Model

To infer the origin of the basement uplift and the onset of the geothermal activity, we inspected field photographs taken during

our three expeditions combined with drone-set Gopro camera pictures taken in January 2016 and 2017. We built photomosaics combining (i) high-resolution images of a drone-mounted Gopro camera (January 2019 campaign), (ii) photographs and videos taken from a drone and from a helicopter with a coupled FLIP DUO thermal camera and Gopro visual camera, and (iii) field mapping data collected with a Juno GPS Handle with the ESRI's Arcpad software. All mapping data were processed with ArcGis© 10.5 of ESRITM. We built the model of genesis and evolution of the dome based on the cartographic data and the analysis of recent evolution of the geothermal activity to precise the evolution steps of the formation of the Dallol dome. For this purpose, we used the freely distributed satellite and aerial images detailed in “Satellite and aerial photographs” section.

RESULTS

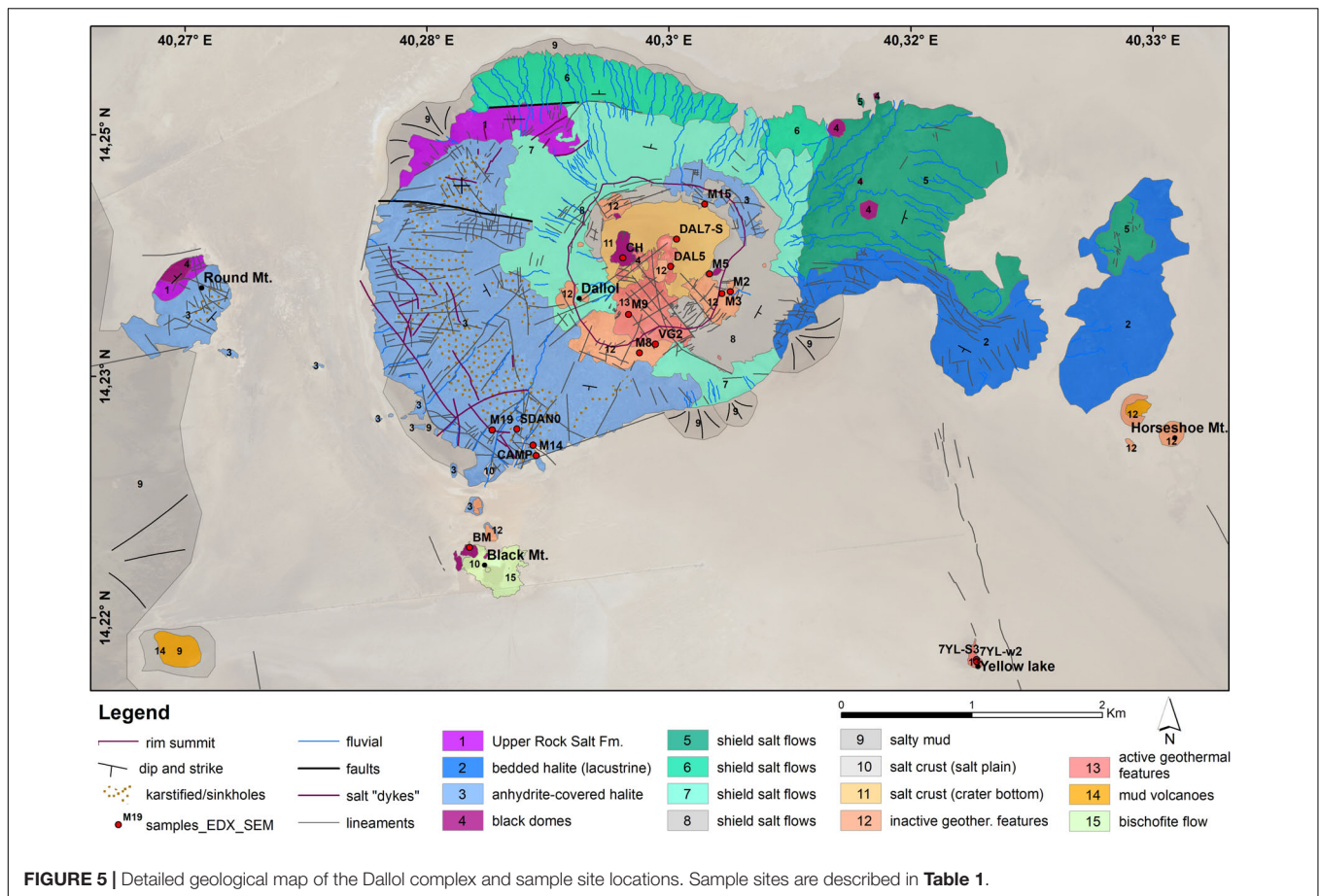
Geological Mapping and Petrographic Characterization of the Dallol Complex

We reconstructed a detailed geological map of the Dallol dome and the adjoining structures (**Figure 5**) based on field data and photo interpretation. We identified fifteen geological units almost exclusively composed of salts. To better characterize some salt units, we conducted a petrography study on selected samples by XRD and SEM, establishing the paragenesis of main mineral phases present (**Table 1** and **Figure 6**). We also mapped several geomorphological features that provided key data on the evolution of the dome, including a fluvial network, lineament patterns (including open fractures, straight canyons, dyke-like structures, and elongated and or aligned sinkholes), karstified/sink-hole areas and the dome crater rim. A combined analysis of both Danakil and Dallol geological maps allowed us to elaborate the geological cross section shown in **Figure 1C**.

The Dallol host rock corresponds to an uplifted basement mainly outcropping in the west and southwest parts of the dome (Franzson et al., 2015) and dipping gently outside (**Figure 5**). Based on our field observations, as well as satellite and aerial photo-interpretation, we differentiate two units of outcropping primary salt deposits. The first deposit (no. 1 in **Figure 5**) consists of black, gray and white bedded halite that outcrops only in the north side of the Round Mountain and in a small corridor on the NW Dallol dome, dipping to the NW in both cases. They probably correspond to the “core” described by Talbot (2008) outcropping in a “window” north of the Dallol mining camp (Dallol point in **Figure 5**). The second primary halite outcropping consists of red bedded halite with minor gypsum, anhydrite and clay interlayers (no. 2 in **Figure 5**). This “upper bedded sequence” (according to Talbot, 2008) overlies unconformably the Dallol core halite, dipping gently outside the Dallol dome and to the SE in the Round Mountain. In the Dallol dome W

⁴https://www.google.es/intl/es_es/earth/

⁵<https://www.malvernpanalytical.com/es/products/category/software/x-ray-diffraction-software/highscore-with-plus-option>



flank and the top NE area around the crater rim, this halite sequence is covered by a white unit of thin, often brecciated, gypsum and anhydrite layers. These are interlayered with unique lacustrine silica-rich marls, diatom-rich white silts and clays (no. 3 “lacustrine deposits” in **Table 1** and **Figure 5**). We carried out additional XRD and SEM analyses of selected anhydrite-gypsum layers of this unit to compare it with similar lacustrine deposits of the southern Afrera Formation outcropping around the Bakili and Afrera lakes (**Figure 6**). Interestingly, although the major phases were calcite and halite for the Afrera Formation samples versus anhydrite for the Dallol samples, the two units showed clear mineralogical similarities. These included the shared presence of calcite, gypsum, muscovite, corrensite/chlorite and hydrated Mg-silicates, possibly stevensite or kerolite as attested by broad peaks in cobalt 2 θ at 23.6° (4.5 Å), 41° (2.5 Å), and 72.6° (1.5 Å) typical of soda lakes (Zeyen et al., 2015). The halite-gypsum-anhydrite Dallol unit is affected by intense karstification, as shown by the occurrence of deep salt canyons (**Figures 3C,D**), caves and sinkholes along the fracture-associated subsurface fluvial network. Fracturation, karstification and the protective role of less-soluble anhydrite beds on underlying halite series result in the formation of the impressive salt canyons’ landscape (**Figure 7**), punctuated by isolated buttes, pinnacles and demoiselles (**Figure 3C**). On top of the dome, the crater-like depression (~1 km diameter, 15 m depth) contains different

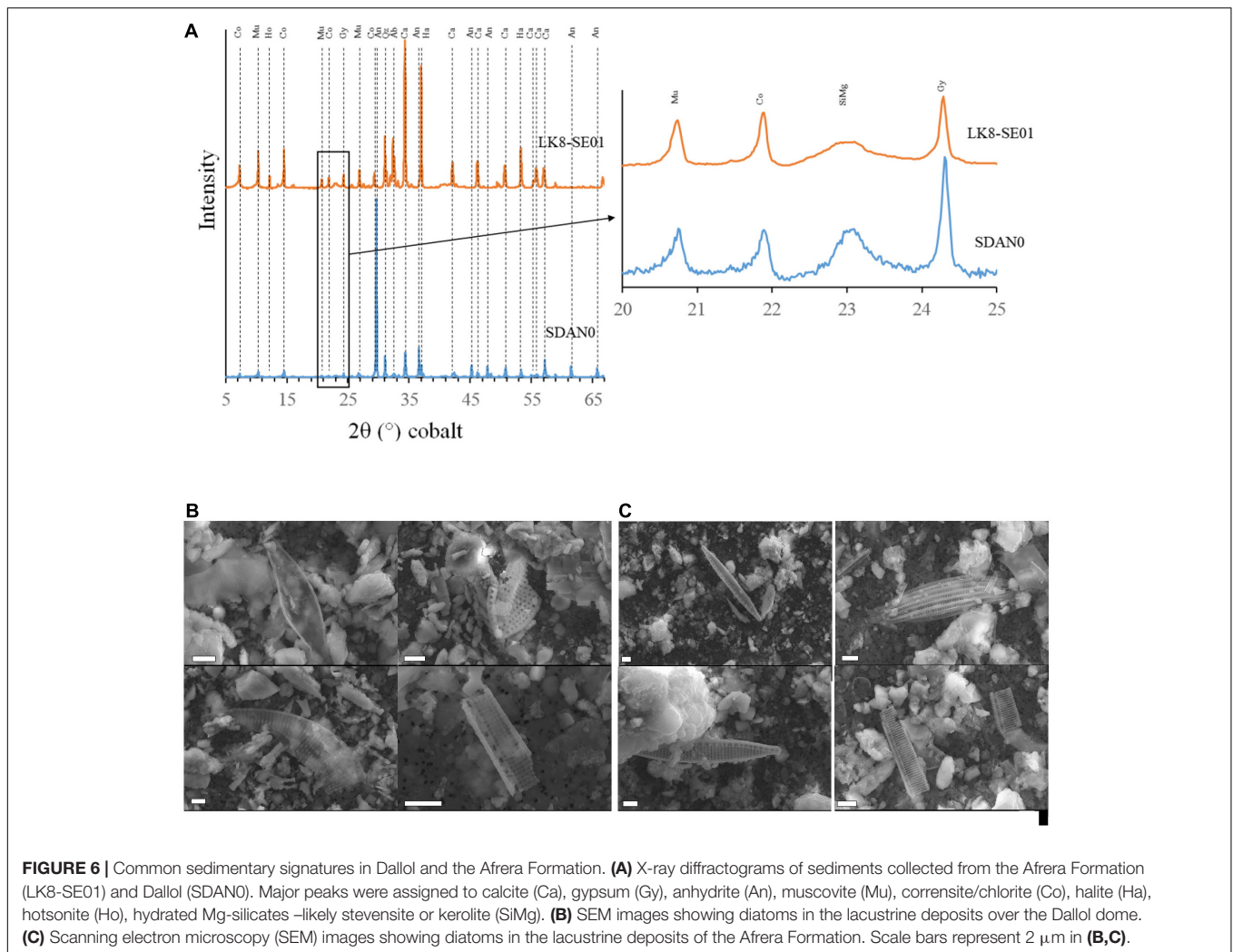
salt deposits and morphologies resulting from recent geothermal activity around the crater rim. The flat bottom of the depression is covered by a salt crust (**Figure 3E**) formed by the evaporation of a temporal lake that repeatedly forms after periodic flooding from both meteoric and/or outflowing of hydrothermal groundwater.

From the crater rim to the uplifted halite basement, the dome is partially covered by salt shields produced by salt flows of low viscosity (Franzson et al., 2015). We identified different fluvial network patterns suggesting several past flowing events. The most ancient one, associated with the most intense fluvial network development, can be seen in the eastern (no. 5 in **Figure 5**) and northern (no. 6 in **Figure 5**) external dome parts. The northern side is also affected by some faulting processes reflecting recent halokinetic and/or tectonic activity. The most recent flows locate around the crater-rim upper part (no. 7–8 in **Figure 5**), with less or no fluvial incision. We observed color differences between these salt shields, reflecting chemical variations between either distinct flowing events or chemical composition evolution during a unique flowing event. Contrasting with the fluency of these deposits, dense dark halite flows with a high content in hematite, known as black domes (Franzson et al., 2015), outcrop in different parts along the Dallol complex (no. 4 in **Table 1** and **Figures 3E–H**, 5). These flows frequently preserve an extrusive morphology (**Figure 3E**), as it can be seen at the bottom of the crater, evoking those of lava flows. In agreement with the high viscosity of these

TABLE 1 | Identification of mineral phases in samples from the Dallol dome and surroundings.

Unit/Paragenesis	Sample name	Brief description	Coordinates	Mineral phases
3 anhydrite covered halite (lacustrine deposits)				
Anhydrite, halite, silica (diatom fragments) and (calcium carbonate)	CAMP SITE	Anhydrite top layer on the Western salt canyons, Dallol dome	14.228576 N 40.29063 E	Ca(SO ₄)
	M19	dusty white soft rock in a dyke or infilling a fracture in the Salt Canyons	14.229637 N 40.28781 E	Ca(SO ₄), NaCl, SiO ₂ , Ca(CO ₃)
	M15	Anhydrite-gypsum lacustrine deposits a top of the bedded halite in salt canyons	14.24521 N 40.302453 E	Ca(SO ₄), K _{0.95} (H ₃ O), NaCl, SiO ₂
	M14	Silt-marly soft, dusty and very light white rock	14.227855 N 40.290853 E	Ca(SO ₄), SiO ₂ , NaCl, Ca(CO ₃)
	SE-01	Silt-marly soft dusty and very light white rock with root bioturbation and diatoms	13.879159 N 40.679978 E	CaCO ₃ Si (e.g., diatoms) Mg-silicate Mn-rich phase (with Ca, Si, Al, and Mg) Fe rich phases (with Si and Al, Mg, and K)
	SDAN0	Light white rock felt from upper bedded halite sequence close to campsite	14.229700 N 40.289514 E	Ca(CO ₃), CaSO ₄ , Mg silicates, or MgAl Si Ca?, diatom fragments
4 black domes				
Halite, hematite (sylvite, anhydrite)	BM	Black salt fragments from the Black Mountain	14.221519 N 40.286261 E	NaCl, Fe ₂ O ₃
	CHOCO	Black salt fragments from the Black dome inside Dallol crater ("chocolate formation")	14.241505 N 40.296815 E	NaCl, Ca(SO ₄), Fe ₂ O ₃ , KCl
12 inactive geothermal features (sulfur emission)				
Native sulfur, anhydrite (halite)	M8	Silt-sized dust around sulfur emission point	14.234953 N 40.297964 E	S, Ca(SO ₄), NaCl
	M2	Sulfur fragments close to an emission point	14.239164 N 40.304218 E	S, Ca(SO ₄), MnO ₂
	M3	Salt-sulfur solidified flow	14.23904 N 40.303653 E	S, Ca(SO ₄)
	M5	Altered salt-sulfur flowing crust	14.240385 N 40.302772 E	S, Ca(SO ₄), Mg _{0.67} Al _{0.33}
	VG2	Salt-sulfur solidified flow	14.235544 N 40.299058 E	S, NaCl, Ca(SO ₄)
13 active geothermal features (dome geothermal salts)				
Halite, brushite (dawsonite)	DAL5	Fragment of brownish salt, top do the dome	14.240908 N 40.300119 E	NaCl, CaPO ₃ (OH) ₂ H ₂ O, NaAl(CO ₃) (OH) ₂
	DAL7-S	Brownish salt crust on top of the Dallol dome	14.240908 N 40.300119 E	NaCl, CaPO ₃ (OH) ₂ H ₂ O
	M9	Salt ball	14.2376 N 40.297208 E	NaCl
13 active geothermal features (bubbling springs, Yellow Lake)				
Carnallite, (halite)	7YL-S3	Salt fragment from the rim of a bubbling pond in the Yellow Lake area	14.213792 N 40.321166 E	KMgCl ₃ (6H ₂ O), NaCl, FeS, MgFe ₂ O ₄ , Na(NO ₃), TiO ₂
	7YL-w2	Wax-like salt fragment from the corner of a bubbling pond in the Yellow Lake area	14.213648 N 40.321188 E	KMgCl ₃ (6H ₂ O), Fe ₂ Si, Ca ₂ MgCr ₂ (SiO ₄), FeSe

Unit numbers and sample names correspond to those on **Figure 5**.



flows (Franzson et al., 2015), they often exhibit hexagonal joints (**Figure 3E'**), indicating retraction after cooling and internal folding. We also observed in these dark salt flows small open pits containing native sulfur. These seem to be remnants of a later degassing after flooding. Likewise, we observed some circular tubes infilled with almost transparent or white halite (**Figure 3E'**). These can be interpreted as the extrusion vent last morphological expression modeled by subsequent compositional evolution of salt flows. As mentioned above, black domes with a similar composition appear in different parts of the Dallol complex. They include the Black Mountain (“BM” sample in **Table 1**) and the Skating Rink, 15 km to the south. In the Black Mountain, geothermalism displays signs of recent explosive activity, as shown by the occurrence of big salt boulders ejected from geothermally active open fissures (**Figure 3G**).

The younger salt deposits result from the recent hydro-geothermal activity involving acidic hot brines. They include a wide variety of morphologies, described in the geothermal features section below. Due to mapping scale constraints, we have differentiated only two map units. The active geothermal

features (no. 13 in **Figure 5**) correspond to those associated with brines and active degassing. Usually colored in white, yellow and brown, they have easily identifiable morphologies and are mainly composed of halite and brushite according to XRD analysis (no. 13, dome geothermal features in **Table 1**). The inactive geothermal features are represented by degraded salt mounds, drilled by degassing vents. The mounds are frequently collapsed and the dissolved halite gives way to the appearance of dusty grounds with predominance of less soluble anhydrite. Native sulfur around degassing vents is also frequently observed (no. 12 “sulfur emissions” in **Table 1** and **Figures 8I,J**).

Bordering Dallol, clay and silt deposits are the remnants of the salt dissolution dragged by the fluvial activity on the dome (no. 9 in **Figure 5**). Beyond the dome, a flat salt crust, mainly composed of halite re-precipitated after flooding events, extends forming the Danakil salt plain (no. 10 in **Figure 5**). Likewise, a salt crust formed by precipitation (and re-precipitation after heavy rainfalls, when a temporary lake can be formed, e.g., **Figure 4B**) of salts from geothermal brines covers the bottom of the Dallol crater depression (no. 11 in

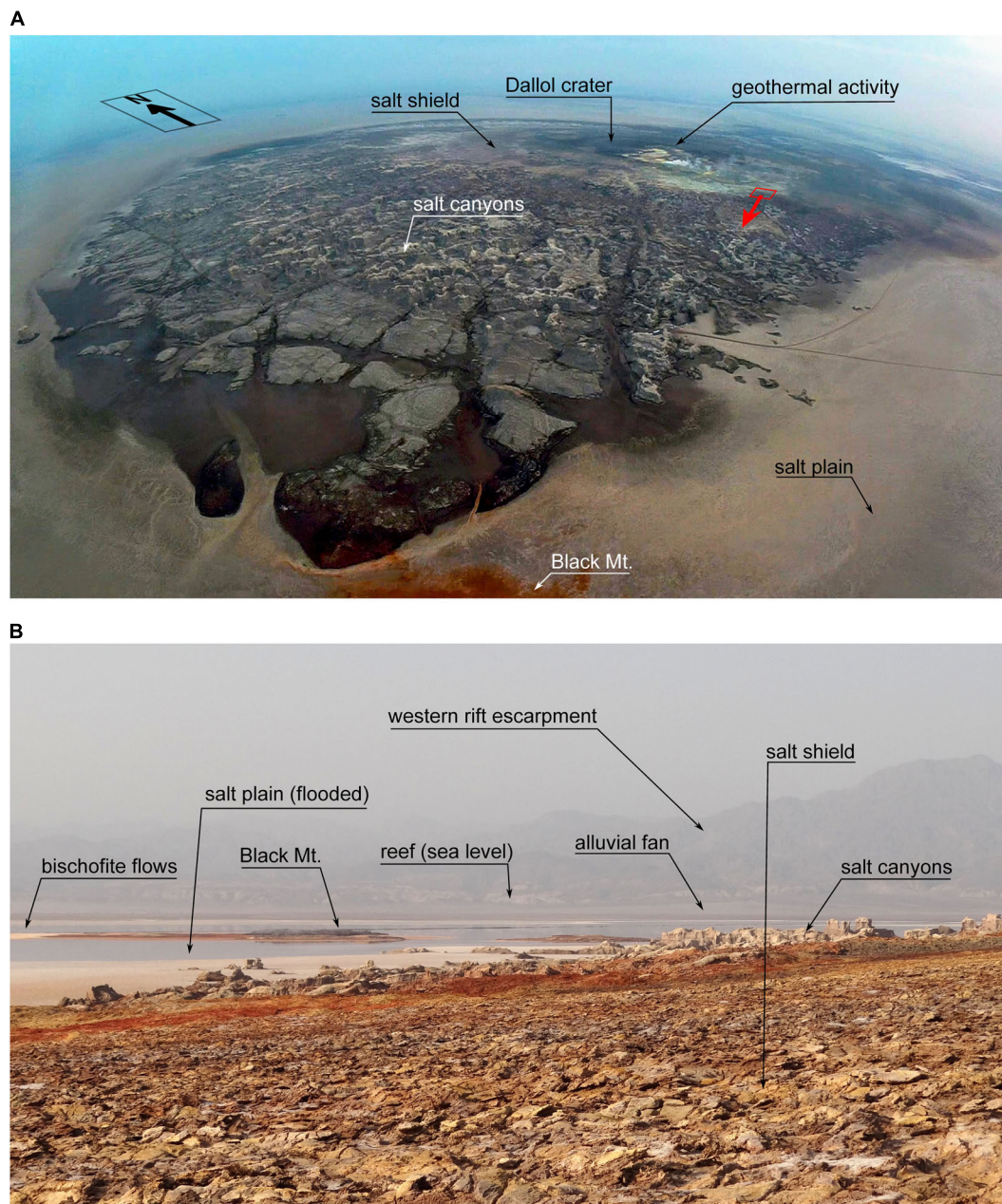


FIGURE 7 | Aerial view of the Dallol dome. **(A)** View taken from the vertical of the Black Mountain to the northeast. **(B)** Opposite ground image taken from the top of the dome to the southwest.

Figure 5). Additional active geothermal features emerge from the salt plain around Dallol at increasing distances. The Yellow Lake (**Figures 3I, 5**) is a brine pool of ca. 40°C bubbling water located 4 km southeast, at 1–2 m below the salt plain ground level. Halite with significant amounts of carnallite and other metal oxides form most of the salt deposits around the main circular pool (no. 13 “bubbling springs” in **Table 1**). Associated with it, a series of smaller ponds align N-S following the rift East-segment inner fault. We identified similar bubbling pools aligned following an E-W direction north of the Round

Mountain, 3.5 km west of the Dallol crater (**Figures 3J, 5**). The Black Lake is also an active small geothermal pond (~15 m diameter, ~10 m depth) located close to the north limit of the Black Mountain and containing an acidic (pH ~3) hot (~70°C) extremely hypersaline (>70%) brine, mainly composed of bischofite (magnesium chloride) (Belilla et al., 2019). The Black Mountain area exhibits frequent massive bischofite flows, which we witnessed in January 2016 and 2019 (no. 15 in **Figures 3F, 5**), coming from several emission centers located close to the southeast Black Mountain limit. This activity and

the resulting deposits are the most changing feature of the Dallol complex, as can be seen in the historical satellite images from the last decades (**Supplementary Video S1**). The Skating Rink is a ca. 300 m-diameter circular structure composed of upturned brown halite beds protruding from the salt plain at 15 km south of the Dallol dome on the way to the Hamedela village (**Figures 1, 3H**). In addition to these structures, we studied three small islands, composed of primary bedded halite similar to that forming the upper-bedded sequence of the western Dallol Salt Canyons, which emerge few meters above the Assale Lake water level (**Figure 1**). The Black Mountain, the Skating Rink and the Assale Islands follow a line along the NW-SE rift that also joins the almost symmetrically located craters of the Maraho and Gada Ale volcanoes, which outcrop 32.7 km in the NNW and 31.8 km in the SSE of Dallol, respectively (**Figures 1A,B**).

Geothermal Features

On the Dallol dome, the youngest salt deposits and morphologies resulting from intense recent hydrothermal activity cover a large part of the southwestern and northern crater rim. Some of these geothermal salt deposits have remained inactive (no. 12 in **Figure 5**) during the last decades, as it can be seen on satellite images, and show different degrees of preservation as compared to twin morphological structures occurring in active areas. From the south crater rim to its center, active geothermal areas (no. 13 in **Figure 5**) broadly extend. A wide variety of geothermal features resulting from salt precipitation of over-saturated brines around hot springs, most of them already described (Franzson et al., 2015), can be identified. Based on field observations we have defined and illustrated the most representative ones in **Figure 8**.

In active geothermal areas (no. 12, **Figure 5**), the most common structures are small salt cones formed around active geysers (**Figure 8A**) or fumaroles (**Figure 8B**) in the cm- to dm- scale although, occasionally, growing to form chimneys or pillars up to 2 m high. Salt cones usually cluster and form flat top terraces associated to acidic brines (**Figure 8C**) or steam grounds (**Figure 8D**), depending on whether salt cones expel water (geysers) or gas (fumaroles). One of the most spectacular morphologies are the salt terraced ponds (**Figures 8E,F**). When they are full of water, they exhibit very low pH values ($\text{pH} \leq 0$) and high amounts of iron, manganese, and sulfur (Belilla et al., 2019) at different oxidation states that color these pools with an impressive green, orange and yellow palette detailed in Kotopoulou et al. (2019). Most of the different delicate salt crystallization processes take place in these areas, some of them being very common, as the mushroom-like salt deposits (**Figure 8G**), while others are very rare, e.g. salt balls (**Figure 8H**).

All these features continuously evolve depending on geothermal activity. Due to their salt composition, they are very soluble and rapidly degrade or disappear in inactive areas (no. 13, **Figure 5**), where only the most insoluble deposits leave remains, such as the native sulfur deposits associated to degassing vents (**Figures 8I,J**).

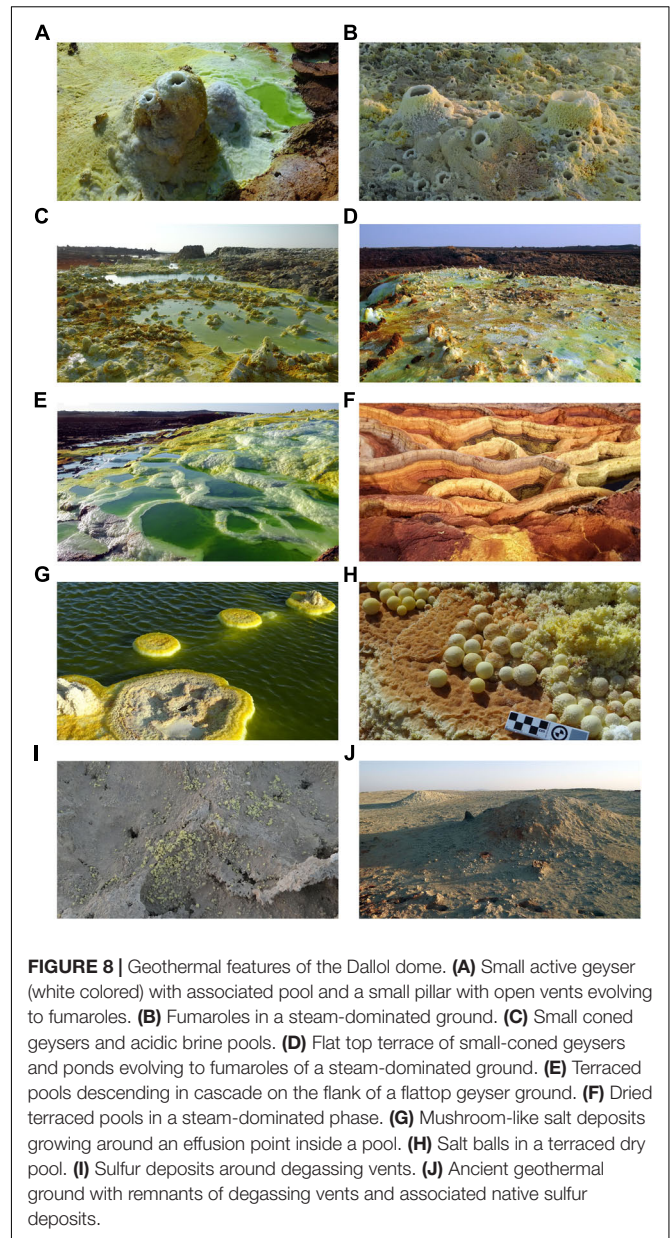


FIGURE 8 | Geothermal features of the Dallol dome. **(A)** Small active geyser (white colored) with associated pool and a small pillar with open vents evolving to fumaroles. **(B)** Fumaroles in a steam-dominated ground. **(C)** Small coned geysers and acidic brine pools. **(D)** Flat top terrace of small-coned geysers and ponds evolving to fumaroles of a steam-dominated ground. **(E)** Terraced pools descending in cascade on the flank of a flattop geyser ground. **(F)** Dried terraced pools in a steam-dominated phase. **(G)** Mushroom-like salt deposits growing around an effusion point inside a pool. **(H)** Salt balls in a terraced dry pool. **(I)** Sulfur deposits around degassing vents. **(J)** Ancient geothermal ground with remnants of degassing vents and associated native sulfur deposits.

Mapping of Geothermal Activity

The hydrogeothermal activity fluctuates rapidly in the dome. During our January 2016 campaign, we mapped a total active area (steam-grounds, fumaroles, pillars, boiling pools, and ponds) within the Dallol rim of 0.038 km², which is less than half of the 0.087 km² estimated from the 2012 geological map (Franzson et al., 2015). However, in January 2017, we measured a very intense geothermal reactivation, with a total new active surface composed of recent white and yellow salt deposits and free water extension coming from active fumaroles and geysers of 0.144 km² (Belilla et al., 2019; Kotopoulou et al., 2019).

To gain insights into the evolution of this highly dynamic activity over a longer time span, we analyzed more than one thousand images from Landsat and Sentinel satellites taken

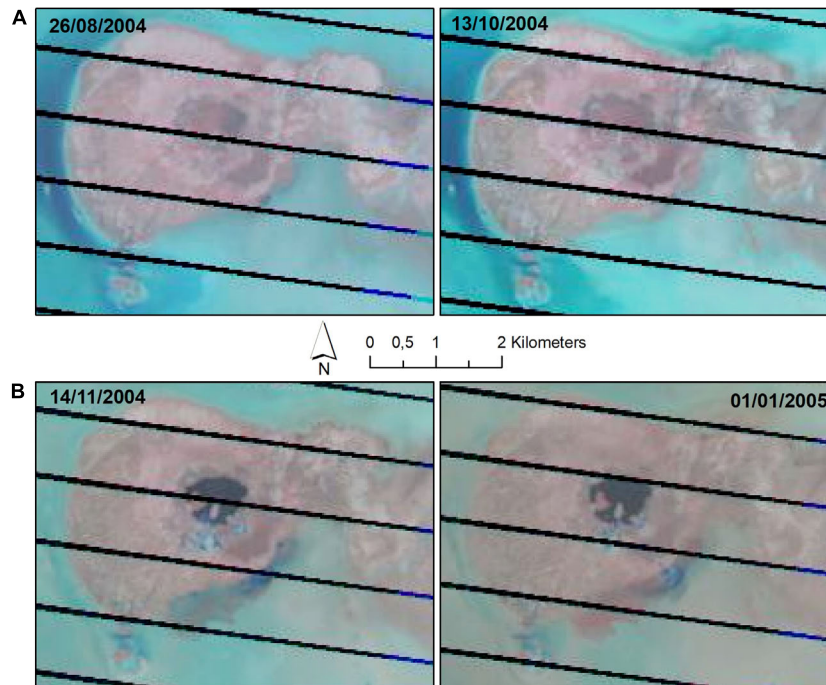


FIGURE 9 | Satellite images showing the 2004 dyke-intrusion event. Landsat 7 (NASA) satellite images over the Dallol dome before **(A)** and after **(B)** the dyke-intrusion event of October 22th – November 4th 2004.

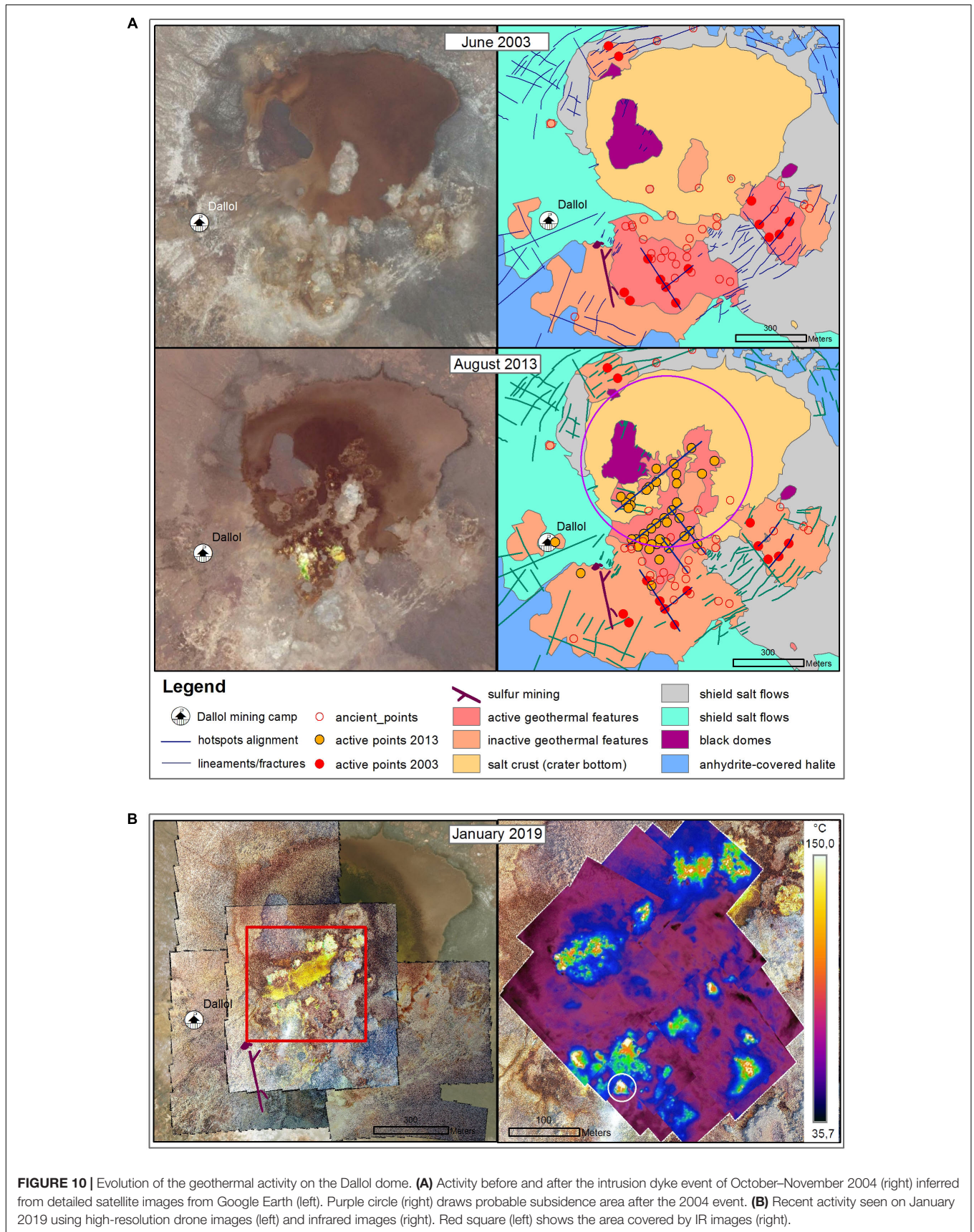
between 1972 and 2019. Despite the low resolution of the oldest Landsat 1–5 images (60 m/pixel between 1972 and 1992), the presence of the Yellow Lake is recognizable. This lake, described as a “brine pool” located southeast of the dome, and the pools at the Round Mountain were already mentioned by Holwerda and Hutchinson (1968). The most remarkable feature in satellite images is the extreme activity and variability around the Black Mountain, 2 km southwest of the Dallol crater. Intense bischofite salt flows are visible with a recurrence of some months, covering periodically large areas around the Black Mountain (e.g., May 1990, December 2000, and January 2013 in **Supplementary Video S1**). By contrast, the geothermal activity was not very intense on the dome between 1972 and 2004, with only some minor changes in the southwestern crater rim. The crater bottom clearly exhibited a central “island,” which corresponds to the highest small hill within the central depression, an inactive salt-mound of geothermal origin already visible in an aerial image of 1968 (Holwerda and Hutchinson, 1968). A strong increase of geothermal activity on the dome is registered in Landsat images between October 13th and November 14th 2004 (**Figure 9**). Large dark areas appeared in the central depression of the dome, while scattered whitish and darker areas extended also along the southwestern part of the rim. To characterize this change in geothermal activity we mapped over the Dallol dome geological map (extracted from **Figure 5**) the active and inactive areas along with the active geothermal points by interpreting two aerial images of Google Earth taken between June 2003 and August 2013 (**Figure 10A**). Both images are compared with a composition of high resolution and IR images

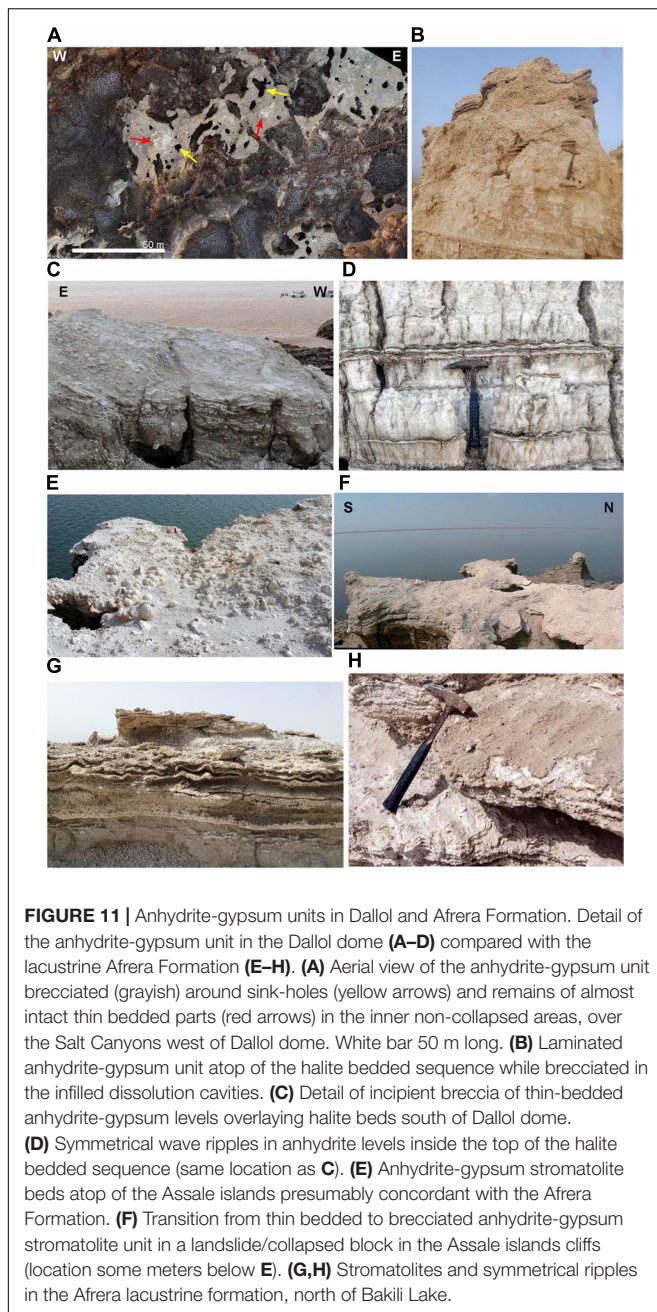
taken with a drone during our latest campaign in January 2019 (**Figure 10B**) to visualize hidden structural patterns in the current extensive active surface.

DISCUSSION

Geological Mapping and Petrographic Characterization: Chronostratigraphic Constraints

Despite the difficulty of dating the salt deposits that form the Dallol dome, the spatial relationships between different salt formations allowed us to establish temporal constraints on the dome origin and evolution. The bedded halite sequence (no. 2 in **Figure 5**) that constitutes the uplifted basement of the dome includes interlayers of gypsum and clays with frequent symmetrical ripple marks (**Figure 11D**) and is covered by a reworked thin anhydrite-gypsum debris unit and, occasionally, marly beds (**Table 1** and **Figures 11B,C**). This chronostratigraphic undefined anhydrite-gypsum unit has lithological and sedimentological similarities with the most recent gypsum deposits of the so-called Afrera Formation of the Danakil depression, which comprises gypsum, marls, diatom-bearing dusty limestones, and clays of lacustrine (salt lake) origin (Varet, 2018; **Figure 2**, number 3 in **Figure 5**). We hypothesize that these two units are the same. During our field trips, we identified some of the best preserved gypsum outcrops of the Afrera formation extending around current Assale, Bakili and





Afrera lakes (Figures 11G,H). According with Brinckmann and Kürsten (1971), this unit would delimit the extension of an ancient massive “Afrera Lake” that encompassed all of them. ^{14}C content-based dating suggests that this sedimentary unit (the “Afrera unit”) formed 5.840 years before present (Brinckmann and Kürsten, 1971). We observed this “Afrera unit” in the form of extensive gypsum stromatolites around Lake Bakili. In addition, we identified similar stromatolitic gypsum layers on two of the small islands in Lake Assale (Figures 11E,F) where the underlying host rock was a bedded halite sequence very similar to the bedded halite sequence outcropping in the salt canyons of the Dallol dome west flank (Figures 11B,C). The Afrera stromatolitic

top gypsum layers appeared brecciated in some areas as it is also the case in the Dallol dome salt canyons. Another example of the Afrera lacustrine deposits covering the bedded halite sequence was mapped by Brinckmann and Kürsten (1971) at the Gada Ale volcano southwest flank, where these lacustrine sediments uplift to form a Dallol-like dome structure, deforming also the overlying lava flows (Figure 1B). Compositional similarities revealed by XRD in anhydrite-gypsum samples from Dallol and the Afrera Formation near Lake Bakili point indeed to the same origin for both units (Figure 6A). Likewise, SEM observations of samples collected from Dallol (Figure 6B) and the Afrera Formation, the last sampled around small lakes between Lakes Bakili and Afrera on the eastern Erta Ale ridge flank (Figure 6C), revealed the presence of abundant diatom frustule fragments that are an important source of the silica detected in all the lacustrine samples (no. 3 in Table 1). Consistently with all these field observations and analyses, we hypothesize that, during the Dallol dome early evolution (Figure 13A), the ancient hypersaline “Afrera” Lake occupied most of the North Danakil basin, extending up to the Dallol area. On what is today the Dallol west flank, bedded gypsum and anhydrite evaporites formed, the remnants of which can be seen today capping the salt canyons (Figure 11A). Fragments of diatom frustules similar to those present in the Afrera Formation were also observed in brine samples collected at a hydrothermal chimney located on the crater south rim in January 2017 (Kotopoulou et al., 2019), which confirm the presence of this lacustrine unit below the geothermal salt deposits outcropping on top of the Dallol dome in this area. The lack of top lacustrine anhydrite layers on the eastern Dallol dome flank can be explained by the asymmetry of the basin and/or the original uplift of an incipient dome structure over the lake level on this side. If the anhydrite and gypsum cover of the bedded halite is indeed coetaneous with the Afrera formation, then the main Dallol dome uplifting and all overlying salt flows and geothermal deposits must have occurred less than ~6000 years ago.

The Black Lake (Figure 3F) has an accurate dating since an Afar inhabitant witnessed its appearance after a phreatic explosion in 1926 (Holwerda and Hutchinson, 1968). The age of the rest of salt units remains unclear but some constraints can be made based on their geometric relations and preservation. The extrusion of the black domes may not be contemporary but, inside the Dallol crater, the morphological preservation, the stratigraphic relation with salt shield flows and the proximity to the over-imposed geothermal features indicate recent extrusion (Figure 3E). The different mapped salt shield flows (no. 5 to 8 in Figure 5) can also be relatively dated according to their relative position around the crater and the different incision degree of the fluvial network. Finally, the most recent deposits are those resulting of the geothermal activity that can be seen currently active or visible in historical satellite images.

Genesis and Evolution of Geothermal Features

Based on observations during our three expeditions and the interpretation of aerial photographic records, we can establish

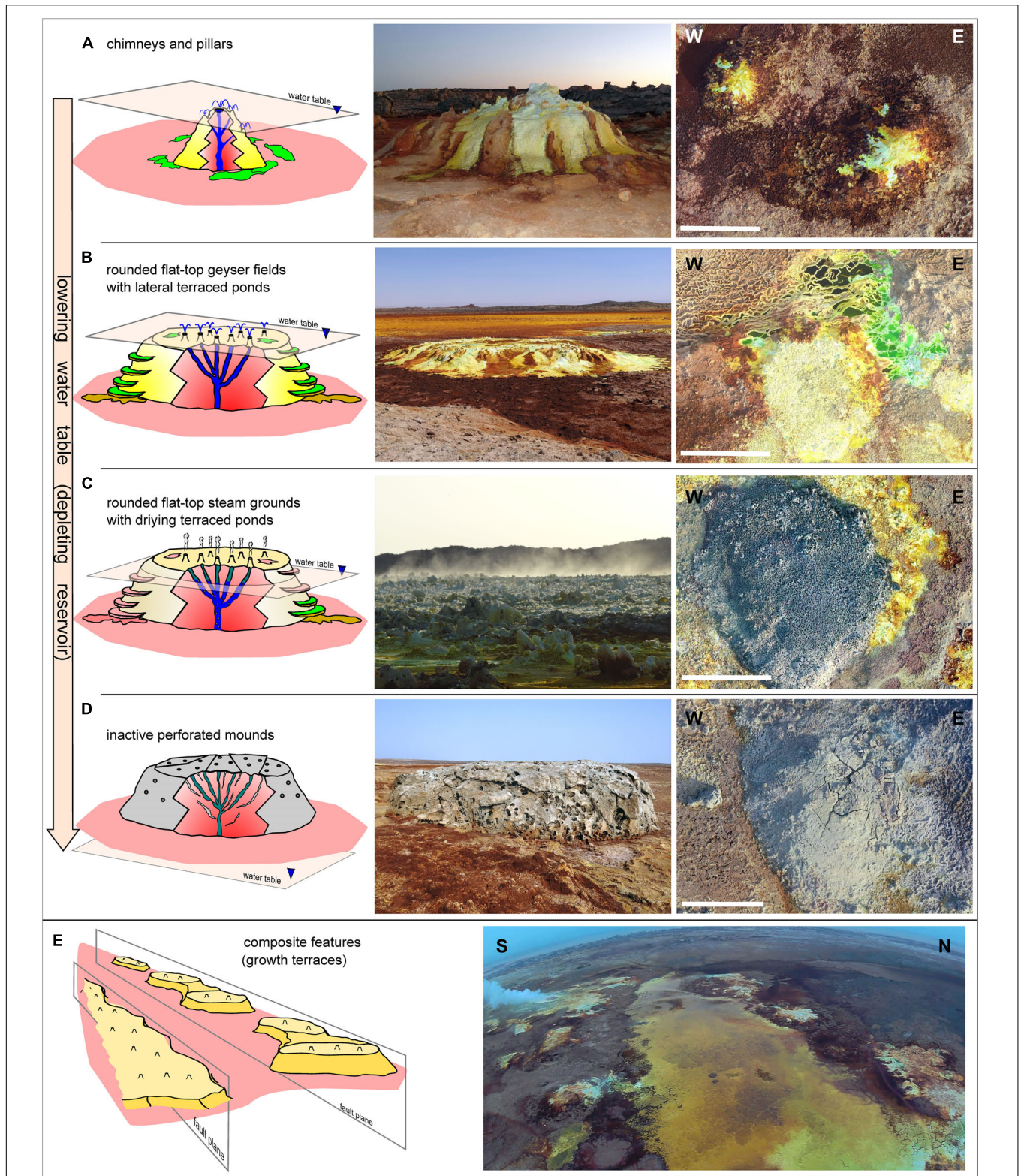
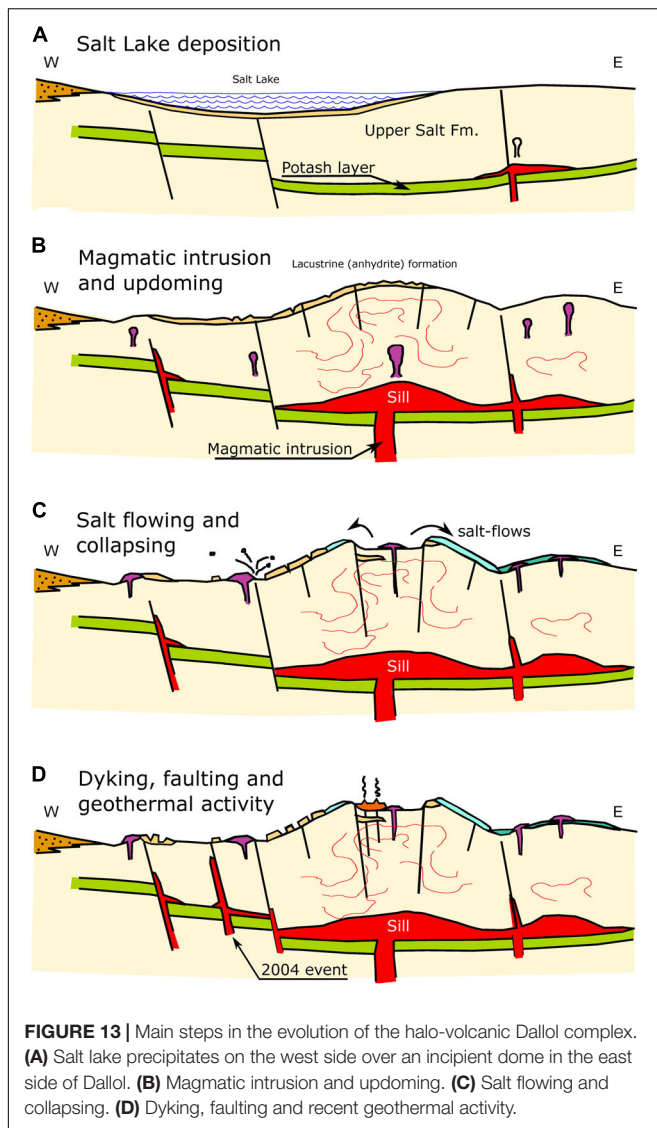


FIGURE 12 | Geomorphological evolution of rounded geothermal features and their relation with the water table level. **(A)** isolated pillars and chimneys. **(B)** Rounded flat-top geyser fields (growth-terraces) and lateral terraced ponds. **(C)** Rounded flat-top steam grounds and associated drying terraced ponds. **(D)** Inactive salt-mounds. **(E)** Merging of geothermal structures to form composite features. Central column: examples of ground photographs of the geothermal features described on the left column. Right column: drone high resolution images of some of the features described on the left (white bar 20 m long).



a model of evolution for the large Dallol rounded geothermal salt deposit related with the water level fluctuation of the reservoirs feeding the geothermal system. First, the activity possibly begins in a single brine emission point, akin to the “circular manifestation” mentioned by Franzson et al. (2015). Salt deposits form by rapid precipitation of cooling hypersaturated fluid around spouter and geyser emission channels, creating white-colored small salt cones (several cm- to dm- scale) and big chimneys or pillars (up to 2 m high; **Figures 8A, 12A**). These circular manifestations are difficult to identify due to subsequent evolution, but aerial and UAV images can evidence this initial step, such as in the ancient aerial photograph from Google Earth of June 2003 shown in **Figure 10A**. This stage can gradually evolve with new small vents opening and forming clusters of hot springs, small cones and geysers. These continuous spouters emit hyperacidic ($\text{pH} \leq 0$), halite-oversaturated brine at a temperature around 108°C (Belilla et al., 2019; Kotopoulou et al., 2019). Degassing steam makes the brine erupt usually a few centimeters

for a few seconds with irregular periodicity. Pillars gradually evolve to irregular white-to-yellow rounded salt mounds around the first emission point (**Figure 12B**). Mound irregular tops evolve into flat topographies that can grow decimeters-to-meters above the ground, depending on the feeding water reservoir piezometric level (Talbot, 2008). Fluids from geysers and spouter hot-springs accumulate on their upper part, forming numerous acidic brine pools (**Figure 8C**), which cascade down the mound flanks and lead to the formation of the spectacular salt terraced ponds that characterize Dallol (**Figure 8E**).

Rather than dying by clogging, as suggested by Talbot (2008), our observations point rather to an evolution of the spring activity related with the water table fluctuation in semi-independent underground reservoirs. As the water table decreases, the dewatering capacity diminishes. Concomitantly, the hydrogeothermal system releases more steam and geothermal gasses, turning geysers and hot-springs into fumaroles (**Figures 8B,D**) and transforming the geyser fields into steam-grounds (**Figure 12C**). The associated ponds progressively disappear, leaving dried terraced pools around the rounded mounds (**Figure 8F**). The geothermal activity ends with the water reservoir depletion. The main cavities then collapse, closing the connection between the hydrogeological system and the surface. The mounds start to undergo dissolution and re-precipitation, and the extensively perforated salt deposits degrade and collapse (**Figure 12D**). The steam-grounds evolve into dusty mounds (“tufa-like” according to Talbot, 2008; **Figure 8J**). This happens once most of the halite is removed by dissolution and the less soluble anhydrite accumulates. The latter comes from the original anhydrite lacustrine deposits overflowed by the salt shield (e.g., the inactive geothermal area in the south of the crater rim) and frequently hosts native sulfur precipitates (no. 12 in **Table 1**) from the last gas-emitting vents (**Figure 8I**).

The Dallol system is highly dynamic, as monitored on site with drone flights in our field campaigns (Kotopoulou et al., 2019; Belilla et al., 2019) and by aerial photographic records provided by historical imagery of Google Earth and satellite images (**Supplementary Video S1**), and can change in a matter of days or weeks. Centimeter-scale changes in the pond water level can be observed in only a few days. When the surface of some Dallol areas dries out, the geothermal activity can start again as new water supplies feed the depleted reservoirs. Thus, old geothermal features can be reactivated and new deposits can overlay ancient ones in a new cycle leading to the adjoining of isolated former emission points. Frequently, these isolated rounded geothermal features can join adjacent circular manifestations along active open fractures, which resemble, at smaller scale, the aligned travertine chimneys of the Lake Abhe at the Ethiopia-Djibouti border (Houssein et al., 2014). The result is the new formation of extensive geyser fields and steam grounds (**Figure 12E**) that constitute large growth geothermal flattop terraces covering extensive parts of the dome top.

Recent Evolution of Geothermal Activity

The most important geothermal activity change detected on historical satellite images took place between October and November 2004 (**Figure 9** and **Supplementary Video S1**). This

increase in geothermal activity is coincident with the seismic activity occurred between October 22th and November 4th interpreted with InSAR interferometry by Nobile et al., 2012 as a faulting event and dyke intrusion fed by a previously unknown 2.4 km-deep magma chamber. Color changes in Landsat images taken in October 13th and November 14th (**Figure 10**) are consequence of the appearance of hydrothermal brines in some areas of the crater south rim, while the crater was flooded and a temporary lake formed. At the same time, dark fan-like areas formed in the salt plain in contact with the dome southeastern side. They likely resulted from the increased humidity and oxidation caused by geothermal brines draining underground from the dome crater lake. This remarkable geothermal activity increase can also be seen clearly in Google Earth historical images before and after the 2004 intrusion event. In June 2003, the geothermal deposits were visible around the crater rim (**Figure 10A**), with the main activity reduced to some points in the S-SW crater rim flanks. Some of these ancient active points can be identified as the “circular manifestations” described by Franzson et al. (2015). The most ancient deposits occurred in the crater central hill and in the southernmost, external part of the geothermal area, where the salt deposits were affected by subsequent degassing. These Dallol southwest salt deposits evolved from highly porous rocks to degraded whitish dusty grounds easily recognizable in aerial images. In these areas, the intense degassing led to the formation of sulfur deposits that were historically exploited (1949–1954) by the Dallol Potash, Magnesium, and Sulfur Mines Ethiopian Company Limited in the vicinity of the Dallol mining village (**Figure 10**). Afterwards, the rights were acquired by the Ralph M. Parsons Company that continued the exploitation between 1954 and 1968 (Holwerda and Hutchinson, 1968; Tadiwos, 2013). After the 2004 intrusion event, the activity remained intense in the center of the dome during the beginning of 2005 and again in 2009 (**Supplementary Video S1**). The high quality satellite image of August 2013 let us to define precisely how the geothermal activity expanded towards the North in several new points, spreading in the crater southwest quadrant (**Figure 10A**). These 2013 new points, visible as “circular manifestations,” followed a main SW-NE alignment (joining at least three nearby active points) and a secondary NW-SE one, drawing a structural controlled pattern. A subsiding process identified on the Dallol dome top by interferometry (Nobile et al., 2012) might have underlined the circular area revealed by the periodical-flooding humidity-induced contrast within the crater (purple circle in **Figure 10A**). The rounded geothermal salt deposits around the main effusion points (circular manifestations) coalesced, leading to the formation of the chimney and pond fields. Although it is difficult to identify the most active outputs in these fields, we were able to visualize the hidden fracturing pattern following SW-NE and SE-NW directions during our January 2019 campaign by infrared imaging using a dual thermal-visible camera FLIR DUO R (160 × 120 pixels thermal and 2 megapixel visible resolution) mounted in a Phantom 4 drone (**Figure 10B**). Calibration of thermal images with *in situ* temperature measurements of control emission points revealed two sites of enhanced thermal activity above the average fluid-emitted surface temperature of

108–110°C. The first of these hot spots showed a calculated surface temperature of ~125°C and the second a temperature exceeding the maximum calibrated limit of the camera (150°C). We estimated a surface temperature for this hot spot of ca. 200°C (**Supplementary Figure S1**). This point (white circle in **Figure 10B**) corresponded to the main degassing point at the origin of the vapor/gas column visible over the dome during the 2019 field trip (**Supplementary Figure S1**).

Dallol Dome Uplifting and Halo-Volcanism

Based in the correlation that we have established between the Afrera Formation and the anhydrite-gypsum unit overlaying the older bedded halite sequence, we present an evolutionary sequence for the Dallol dome growing process (**Figure 13**). The initial step (**Figure 13A**) was the precipitation of the gypsum-anhydrite layers of the Afrera Formation around 6000 years ago. The ancient lake extended and covered an area that included the current Afrera, Bakili and Assale Lakes from south to north of the Danakil depression as reflected by the extension of the Afrera gypsum layers, located at an altitude between 105 m bsl and 120 m bsl.

According to digital elevation models, the current position of these anhydrite lacustrine deposits on the Dallol dome is between 110 m bsl (dome base) and 80 m bsl (dome top). That difference would have been the result of a second step (**Figure 13B**) of uplifting along with intense fracturation triggered by the migration of melted material from a shallow magmatic chamber located at 2.4 km beneath the Dallol dome, as hypothesized by Nobile et al. (2012). According to Warren (2015c), the magma could have intruded, forming a sill over the 1 km-deep, 2 to 10 meters thick, potash level inferred from South Dallol drill cores (**Figure 1C**; ERCOSPLAN, 2011). The halokinetic processes involved in the magma-salt deposit interaction would have caused the uplift and deformation of the overlying salt sequence and the subsequent radial fracturing. The bedded halite uplift was followed by fluvial incision and salt dissolution. Witnesses of this karstification process can be seen today as salt-dykes, fractures and aligned sinkholes that develop on the anhydrite-gypsum lacustrine layers atop of the unit (**Figure 5**). Our interpretation is that the dissolution and karstification of the halite beds by meteoric water infiltration across the fracture network led to the remobilization of the thin-bedded overlaying anhydrite-gypsum unit. A sample collected in one salt canyon dyke (M9, **Table 1**) showed similar mineral paragenesis to that of Afrera Formation samples (M14, M15, and Camp Site; **Table 1**). Some examples of the karst collapse-associated breccia process can be seen today around the Assale islands, where the top, well-bedded upper layers of stromatolitic gypsum-anhydrite (**Figure 11E**) form the most frequent debris-dominated facies over the collapsed, landslided salt blocks around the island cliffs. Well-preserved, stratified gypsum layers occur in the inner preserved halite succession parts (the whitest colored areas furthest from the dark sink-holes in **Figure 11A**), while a completely brecciated facies can be seen in the proximity of the sink-holes (**Figures 11B,F**). According to our hypothesis, the uplifting process started on

the Dallol eastern side before the deposition of the Afra lacustrine deposits, which are absent in the east. The uplifting process might have then migrated to the western side once the Afra lacustrine deposits had formed on the main Dallol dome structure and Round Mountain.

In a third step (**Figure 13C**), the interaction between the magma and the URS halite would have produced geothermal fluids derived from salt dehydration and interaction with magmatic and percolating meteoric waters. The geochemistry of thermal waters in the Dallol area certainly results from the influence of this magma intrusion and its interaction with meteoric groundwater. These interactions would promote salt melting and eruption through open fractures acting as vents, in one or more events, leading to the salt-shield covers visible today and contributing to build up the Dallol dome. After extrusion, the accommodation of the empty space on top of the dome led to the formation of the circular lineament pattern seen around the crater rim, including likely normal faults (not easily identifiable in the field due to the geothermal salt deposits covering the halite bedded unit). That would have led to the crater collapse and the formation of the top central depression and dyke-like fissures infilled with sulfur rich salt-flows associated to the main geothermal areas of northwest and southeast parts of the rim. Similar structures have been also described in ancient hydrothermal vent complexes (e.g., Jamtveit et al., 2004; Planke et al., 2005; Hansen, 2006; Omosanya et al., 2018). In this sense, the Dallol complex structure could be considered as a dome plus a salt volcano originating from halo-volcanic eruptions superimposed on the former dome stage, both forming part of a hydrothermal vent complex associated with an intrusive magmatic deep system. Despite the absence of classical volcanic materials, the effusion of melted salts is a physical mechanism of emplacement similar to that of lava flows in conventional volcanic areas. It contributed to the built up of the Dallol edifice which, in its present form of salt volcano, can be considered as the result of halo-volcanic processes, in a wide sense of volcano definition (Borgia et al., 2010).

In the last step (**Figure 13D**), the dome evolution reached a relatively calm phase -its current stage- in which dewatering and degassing drive the geothermal activity, sometimes accompanied by episodes of explosive manifestations (e.g., Black Lake appearance in 1926 or intense geyser activity of Yellow Lake in 2005). Dyke intrusion events and earthquakes as those in October – November 2004 are the most recent reminders of the active rifting process.

Our interpretations concur with the idea that the recent geological activity in Dallol constitutes a halo-volcanic precursor of a future *bona fide* volcano as previously proposed by Nobile et al. (2012). It would be similar to the volcanoes disposed along the rifting direction, e.g., Maraho to the north, or Gada Ale (Kebrit Ale) to the south, likely as a consequence of the anticlockwise rotation of the Danakil block described by Reilinger and McClusky (2011). As mentioned above, a structure located 3 km southwest of the Gada Ale volcano crater, 33 km south of Dallol and close to the Assale Lake

south coastline (**Figure 1B**), might be a good analog of the future Dallol evolution. This 100 m-uplifted salt dome -of 2 km diameter, exhibits curvilinear faults, dissolution processes and some basaltic dykes (Barberi and Varet, 1970), showing halokinetic and magmatic processes similar to those of Dallol, as well as salts interlayered by Quaternary lava flows. It likely provides a contemporary image of the expected future evolution of the Dallol complex domed salt-volcano.

Hydrogeothermal Model of Dallol

The different morphologies present in Dallol can only be explained by the interaction of different processes, in particular the magma intrusion, halokinesis and hydrothermal activity (Detay, 2011) but also tectonics and seismicity playing a role. Considering the geological context of the Danakil, the main aquifers are located in the basement that hosts the halite succession filling the depression. The Jurassic Adigrat sandstones and Antalo limestones are the main hydrogeological units that drive the infiltration of meteoric waters from the Ethiopian plateau to the bottom of the Danakil, as can be seen in the geological cross section (**Figure 1C**). This is also facilitated by faulting associated with the rifting process (Varet, 2010). The presumed depth of this aquifer beneath the Dallol dome is over 2 km, i.e., a depth similar to that of the Dallol magma chamber. The halite filling the depression is a sealing unit overlaying the Jurassic aquifer, which can only connect with the surface through recent fractures opened across the ductile salt deposits. Recent open fractures are indeed observable in the halite infilling, likely forced by magmatic intrusion (**Supplementary Figure S2**). This intrusion might seal the new fractures preventing deep-water outflows along the impervious overlaying salt deposits more than 2 km thick. Therefore, although a connection of the surface with the Jurassic aquifers is possible (or even with the Quaternary alluvial fans on the western escarpment by a transversal structure passing through Dallol), we think that most of the water likely comes from the infiltration of: (i) direct rainfall over the dome; and/or (ii) rainfall in the Ethiopian plateau and Danakil alps and periodical flooding of the Danakil depression (e.g., **Figure 4**). Differences in the potentiometric surface of the geothermal emission centers on the dome and surroundings (e.g., Round Mountain, Black Lake, and Yellow Lake) suggest the prevalence of independent reservoirs rather than a shared deep aquifer.

The current geothermal activity on the Dallol dome is largely dominated by gas and steam emissions. Nevertheless, episodic outflows of hyperacidic and salt-hypersaturated waters drive the precipitation of halite around the emission points, creating different geothermal features. As described in our geothermal feature evolution model (**Figure 12**), the coalescence of these rounded structures around hot springs can produce salt deposits with a flat table-like morphology. On their front, down-flowing fluids leave salt precipitates, which form terraced ponds further extending the lateral flat-table accretion. The height of these flat terraces can vary by a few meters. Likewise, height differences can be observed among terraces from the main active area in the

crater south rim and in the crater-bottom NE-SW-aligned rounded features. In our opinion, these elevation differences are most likely due to distinct potentiometric surfaces of the groundwater in small independent reservoirs associated with distinct fractures instead of a unique deep aquifer that would have a generalized and stable potentiometric water head below Dallol. Geophysical analyses of thermal, seismic, and acoustic spectrograms also show different events related with the circulation of fluids, supporting the hypothesis of an independent behavior of each rounded group of geysers and fumaroles (Carniel et al., 2010).

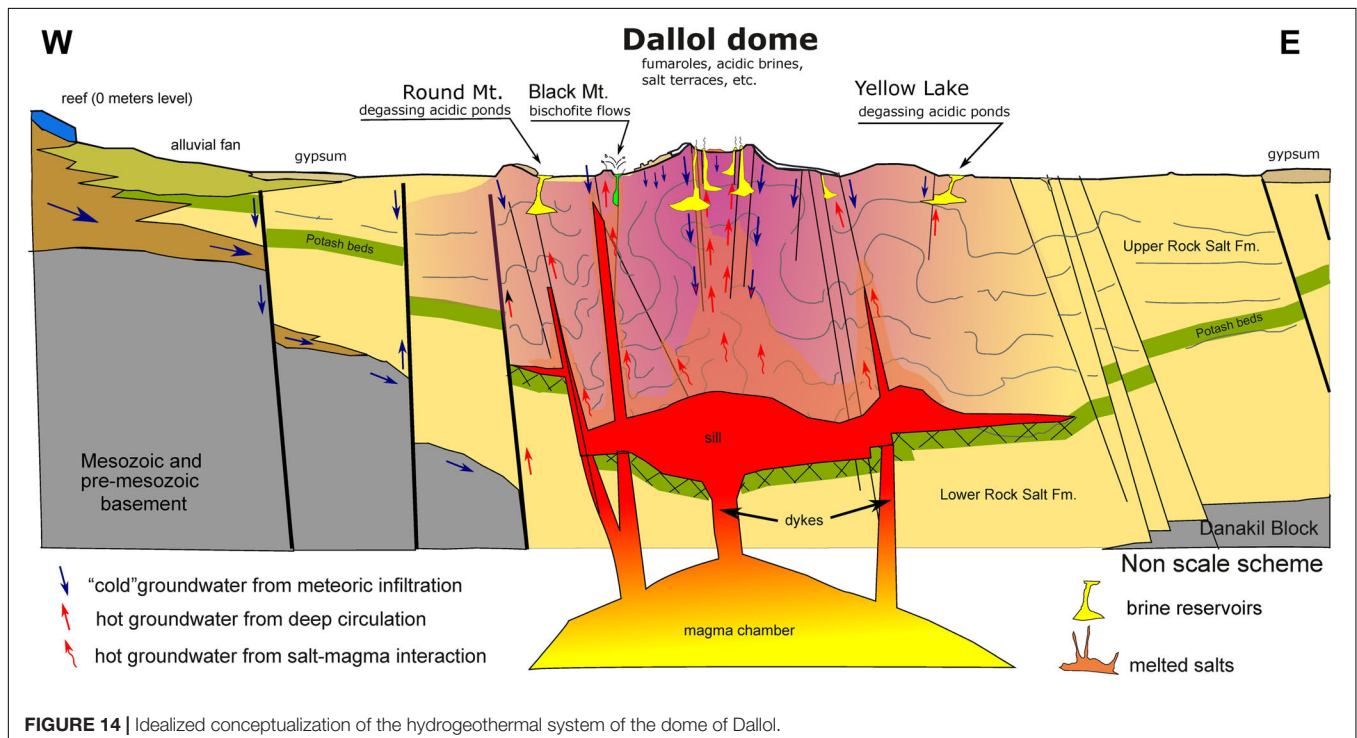
The thermal spring water δD isotope values are similar to those of local meteoric water (-21‰ to -8‰ vs. V-SMOW) with more positive values of the $\delta^{18}O$ ($+5\text{‰}$ to $+8\text{‰}$ vs. V-SMOW), which indicates an interaction with underlying evaporites and basaltic flows (Kotopoulou et al., 2019). The ^{18}O content of the Dallol hot-springs shows an enrichment with respect to the value for meteoric water due to high temperature isotopic exchanges with host rocks (Gonfiantini et al., 1973). In this context, we hypothesize that the dissolution of underlying evaporites may be at the origin of semi-independent reservoirs related with fractures along which fluids circulate (Figure 14). The intense degassing process in the geothermal area leads to the development of high-porosity salt deposits during the water-reservoir depletion process. The most ancient salt deposits are completely perforated by gas outlets (Figure 12C), often leading to their complete collapse (Figure 12D). These areas of high permeability are susceptible to meteoric water infiltration deep into the ground through connecting fractures, thus feeding small reservoirs formed by geothermally induced salt dissolution around the

fractures. Heated at depth, meteoric water would mix with geothermal fluids derived from chemical reactions between salts and magmatic fluids ascending also by the fracturing network over the geothermal area (Holwerda and Hutchinson, 1968; Hovland et al., 2006; Franzson et al., 2015; Warren, 2015c). In this sense, gypsum and other primary salts present in Dallol, including bischofite and carnallite, can be altered at high temperatures and release water (e.g., gypsum buried at 700 m depth and a temperature of $45^{\circ}C$ transforms into anhydrite, releasing 20% of water; MacDonald, 1953). Buried salts interact with the relatively shallow, high temperature magmatic fluids rich in acidic gases (CO_2 , SO_2 , and H_2S) around the Dallol sills and intrusion dykes. This interaction leads to the formation of the hypersaturated anoxic acidic brine that springs up in the Dallol dome. Hydrothermal cavities filled with brines and pressurized gases can also lead to explosive hydrothermal activity (Warren, 2015c).

CONCLUSIONS

During January 2016, 2017, and 2019 we conducted three multidisciplinary campaigns in the Danakil depression, Afar Province (Ethiopia) to study the polyextreme geothermal field of Dallol and shed light on the origin and evolution of the Dallol dome. Using different field and laboratory analyses, we have reached the following goals:

- We have constructed an E-W geological cross-section of the Danakil depression through the Dallol dome and a detailed geological map of the Dallol dome and related structures, including geothermal features and



relevant geomorphological information like the fluvial network, lineaments, and sinkholes/karstified areas. Based on differences in the development of the fluvial network, we inferred the presence of different events of shield salt flows covering de dome.

- We present a petrological characterization of selected salt units by X-ray diffraction, X-ray spectrometry and SEM. Comparative results along with field observations allowed us to infer the common origin of the anhydrite-gypsum unit of the Dallol dome and the Afrera Formation, dated ca. 6000 years ago.
- Based on field observations over three campaigns and with the help of aerial drone images we propose an evolutionary model of the highly dynamic Dallol geothermal features (hot-springs, geysers, chimneys, and pools, etc.) related to the water level fluctuations on reservoirs that feed them, from their origin to their decay.
- We have studied the evolution of the geothermal activity of the dome in recent years with the use of satellite images and found a clear connection between the dyke intrusion event of 2004 and the recent increase in geothermal activity. This event is associated with the reactivation and migration of the geothermal activity towards the north and the opening of new fractures that control the current distribution of active geothermal points.
- We propose a more comprehensive model of the long-term evolution of the Dallol complex with regard to previous ones (Talbot, 2008; Darrah et al., 2013; Franzson et al., 2015; Warren, 2015c). In particular, we present evidence for a recent origin of this structure after the deposition of the Afrera lacustrine formation before uplifting ca. 6000 years ago. The Dallol dome is a complex structure formed by the combination of an uplifted basement (dome) plus a series of superimposed salt flows and geothermal deposits (halo-volcanism) both forming part of a hydrothermal vent complex associated to an intrusive/magmatic deep system. Accordingly, the restrictive definition of a volcano as implying molten silicate rocks should be revised to accommodate different compositions of other eruptive melted rocks such as in the specific case of halo-volcanic phenomena occurring in Dallol.
- We propose a new hydrogeothermal conceptual model for Dallol involving interactions between meteoric water (rainfall and flooding infiltration), magmatic fluids and dewatering of hydrated salts due to shallow magmatic activity. These fluids accumulate in independent reservoirs that are connected with the surface by new fractures opened by tectonic-seismic activity that locally reactivate the geothermal activity.

DATA AVAILABILITY STATEMENT

The datasets generated for this study are available on request to the corresponding author.

AUTHOR CONTRIBUTIONS

JL-G, PL-G, and DM designed and supervised the research. PL-G and OG organized the scientific expeditions. JL-G, PL-G, DM, and KB collected the samples and took measurements *in situ*. JL-G carried out geological and geothermal activity mapping. OG planned mapping flights, piloted the drone, and took aerial and IR photographs. KB performed XRD, SEM, and EDX analyses. JL-G wrote the manuscript, with input from DM, PL-G, and KB. All authors read and approved the manuscript.

FUNDING

This research was funded by the CNRS recurrent annual funding, the CNRS program TELLUS INTERRVIE, and the European Research Council under the European Union's Seventh Framework Program to PL-G (ERC Grant Agreement 322669).

ACKNOWLEDGMENTS

We thank Jean-Marie Hullot (in memoriam), Françoise Brenckmann, and the Fondation Iris (Fondation de France) for funding our 2016 field trip, and the Mamont Frederik Paulsen Foundation for financing the 2019 expedition. We are grateful to Luigi Cantamessa for the *in situ* logistics and discussions about local history. We also thank Anabel López-Archilla, Juan Manuel García-Ruiz, Electra Kotopoulou, Jodie Belilla, and Bernadette Gilbertas for help and discussions during field trips, Jacques Barthélémy for logistics and field support, Nicolas Bellahsen for who provided us with the geological maps of the CNR-CNRS Afar Team, and the editor and the reviewers for constructive comments. We acknowledge Abdul Ahmed Aliyu and the Afar authorities for local assistance as well as the Ethiopian army and the Afar police for providing security.

SUPPLEMENTARY MATERIAL

The Supplementary Material for this article can be found online at: <https://www.frontiersin.org/articles/10.3389/feart.2019.00351/full#supplementary-material>

FIGURE S1 | Example of calibration of IR image based in field temperature measurements of three sample points (DAN006, 9DA2 and 9DA3A) and inferred hotspot1 and hotspot2 temperature.

FIGURE S2 | Recent open fractures in the salt plain, west of the Black Mountain, likely related with the dike intrusion event of November 2014. **(A)** General view over the Black Mountain (dark halite outcrop in the lower left). **(B)** Detail of the open fractures. Photographs taken from helicopter flight during January 2019 campaign.

VIDEO S1 | Evolution of the geothermal activity on Dallol complex seen from Landsat and Sentinel satellite images between 1972 and 2019.

REFERENCES

- Barberi, F., Borsi, S., Ferrara, G., Marinelli, G., Santacroce, R., Tazieff, H., et al. (1972). Evolution of the Danakil depression (Afar, Ethiopia) in light of radiometric age determinations. *J. Geol.* 80, 720–729. doi: 10.1086/627797
- Barberi, F., and Varet, J. (1970). The Erta Ale volcanic range (Danakil depression, Northern Afar, Ethiopia). *Bull. Volcanol.* 34, 848–917. doi: 10.1007/BF02596805
- Bastow, I. D., Booth, A. D., Corti, G., Keir, D., Magee, C., Jackson, C. A. L., et al. (2018). The development of late-stage continental breakup: seismic reflection and borehole evidence from the Danakil Depression, Ethiopia. *Tectonics* 37, 2848–2862. doi: 10.1029/2017TC004798
- Behle, A., Makris, J., Baier, B., and Delibassis, N. (1975). Salt thickness near Dallol (Ethiopia) from seismic reflection measurements and gravity data. *Afar Depress. Ethiop.* 1, 156–167.
- Belilla, J., Moreira, D., Jardillier, L., Reboul, G., Benzerara, K., López-García, J. M., et al. (2019). Hyperdiverse archaea near life limits at the polyextreme geothermal Dallol area. *Nat. Ecol. Evol.* 3, 1552–1561. doi: 10.1038/s41559-019-1005-0
- Bonatti, E., Cipriani, A., and Lupi, L. (2015). *The Red Sea: The Formation, Morphology, Oceanography and Environment of a Young Ocean Basin*, eds N. M. A. Rasul, and I. C. F. Stewart. Heidelberg: Springer-Verlag, 29–44. doi: 10.1007/978-3-662-45201-1
- Bonatti, E., Emiliani, C., Ostlung, G., Rydell, H., Ostlund, G., and Rydell, H. (1971). Final desiccation of the Afar Rift, Ethiopia. *Science* 172, 468–469. doi: 10.1126/science.172.3982.468
- Borgia, A., Aubert, M., Merle, O., and van Wyk de Vries, B. (2010). “What is a volcano?” in *What Is a Volcano?: Geological Society of America Special Paper 470*, eds E. Cañon-Tapia, and A. Szakács, (Boulder, CO: Geological Society of America), 1–9. doi: 10.1130/2010.2470(01)
- Brinckmann, J., and Kürsten, M. (1971). Stratigraphie und Tektonik der Danakil-Senke (NE-Aethiopien). *Beih. Geol. Jb.* 116, 5–86.
- Carniel, R., Jolis, E. M., and Jones, J. (2010). A geophysical multi-parametric analysis of hydrothermal activity at Dallol, Ethiopia. *J. Afr. Earth Sci.* 58, 812–819. doi: 10.1016/j.jafrearsci.2010.02.005
- Cavalazzi, B., Barbieri, R., Gómez, F., Capaccioni, B., Olsson-Francis, K., Pondrelli, M., et al. (2019). The Dallol geothermal area, northern Afar (Ethiopia) – an exceptional planetary field analog on earth. *Astrobiology* 19, 553–578. doi: 10.1089/ast.2018.1926
- CNR-CNRS Afar Team (1973). Geology of northern Afar (Ethiopia). *Rev Geogr Phys Geol Dyn* 15, 443–490.
- Collet, B., Taud, H., Parrot, J. F., Bonavia, F., and Chorowicz, J. (2000). A new kinematic approach for the Danakil block using a Digital Elevation Model representation. *Tectonophysics* 316, 343–357. doi: 10.1016/S0040-1951(99)00263-2
- Corti, G., Bastow, I. D., Keir, D., and Pagli, C. (2015). “Rift-related morphology of the Afar Depression,” in *Landscapes and Landforms of Ethiopia*, ed. P. Billi, (Dordrecht: Springer Science+Business Media), 251–274. doi: 10.1007/978-94-017-8026-1
- Darrah, T. H., Tedesco, D., Tassi, F., Vaselli, O., Cuoco, E., and Poreda, R. J. (2013). Gas chemistry of the Dallol region of the Danakil Depression in the Afar region of the northern-most East African Rift. *Chem. Geol.* 339, 16–29. doi: 10.1016/j.chemgeo.2012.10.036
- Detay, M. (2011). Le DALLOL revisité: entre explosion manifestations hydrothermales et halocinèse. *Lave* 151, 7–16. doi: 10.13140/2.1.2982.4642
- Eagles, G., Gloaguen, R., and Ebinger, C. (2002). Kinematics of the Danakil microplate. *Earth Planet. Sci. Lett.* 203, 607–620. doi: 10.1016/S0012-821X(02)00916-0
- Edelmann, J., Roscoe, R., and Roscoe, R. (2010). “Volcano tourism in Ethiopia and the Danakil Rift Zone,” in *Volcano and Geothermal Geotourism, Sustainable Geo-Resources for Leisure and Recreation*, eds P. Erfurt-Cooper, and M. Cooper, (Abingdon: Taylor and Francis), 59–67.
- ERCOSPLAN (2010). *Technical Report and Current Resource Estimate*. Danakil Potash Deposit, Afar State/Ethiopia. Project Reference: EGB 08–024. Erfurt: ERCOSPLAN.
- ERCOSPLAN (2011). *Preliminary Resource Assessment Study*. Danakil Potash Deposit, Afar State/Ethiopia. Erfurt: ERCOSPLAN.
- Franzson, H., Helgadóttir, H. M., and Óskarsson, F. (2015). “Surface exploration and first conceptual model of the Dallol geothermal area, northern Afar, Ethiopia,” in *Proceedings World Geothermal Congress 2015*, Melbourne, 11.
- Gonfiantini, R., Borsi, S., Ferrara, G., and Panichi, C. (1973). Isotopic composition of waters from the Danakil depression (Ethiopia). *Earth Planet. Sci. Lett.* 18, 13–21. doi: 10.1016/0012-821X(73)90028-9
- Hansen, D. M. (2006). The morphology of intrusion-related vent structures and their implications for constraining the timing of intrusive events along the NE Atlantic margin. *J. Geol. Soc.* 163, 789–800. doi: 10.1144/0016-76492004-167
- Holwerda, J. G., and Hutchinson, R. W. (1968). Potash-bearing evaporites in the Danakil area, Ethiopia. *Econ. Geol.* 63, 124–150. doi: 10.2113/gsecongeo.63.2.124
- Houssein, B., Chandrasekhar, D., Chandrasekhar, V., and Jalludin, M. (2014). Geochemistry of thermal springs around Lake Abhe, Western Djibouti. *Int. J. Sustain. Energy* 33, 1090–1102. doi: 10.1080/14786451.2013.813027
- Hovland, M., Rueslåtten, H. G., Johnsen, H. K., Kvamme, B., and Kuznetsova, T. (2006). Salt formation associated with sub-surface boiling and supercritical water. *Mar. Pet. Geol.* 23, 855–869. doi: 10.1016/j.marpetgeo.2006.07.002
- Hutchinson, R. W., and Engels, G. G. (1970). Tectonic significance of regional geology and evaporite lithofacies in northeastern Ethiopia. *Philos. Trans. R. Soc. A Math. Phys. Eng. Sci.* 267, 313–329. doi: 10.1098/rsta.1970.0038
- Hutchinson, R. W., and Engels, G. G. (1972). Tectonic evolution in the southern Red Sea and its possible significance to older rifted continental margins. *Geol. Soc. Am. Bull.* 83, 2989–3002.
- Jamtveit, B., Svensen, H., Podladchikov, Y. Y., and Planke, S. (2004). Hydrothermal vent complexes associated with sill intrusions in sedimentary basins. *Geol. Soc. Spec. Publ.* 234, 233–241. doi: 10.1144/GSL.SP.2004.234.01.15
- Jaramillo-Vogel, D., Foubert, A., Braga, J. C., Schaegis, J.-C., Atnafu, B., Grobety, B., et al. (2018). Pleistocene sea-floor fibrous crusts and spherulites in the Danakil Depression (Afar, Ethiopia). *Sedimentology* 66, 480–512. doi: 10.1111/sed.12484
- Keir, D., Bastow, I. D., Pagli, C., and Chambers, E. L. (2013). The development of extension and magmatism in the Red Sea rift of Afar. *Tectonophysics* 607, 98–114. doi: 10.1016/j.tecto.2012.10.015
- Kotopoulou, E., Delgado Huertas, A., Garcia-Ruiz, J. M., Dominguez-Vera, J. M., Lopez-García, J. M., Guerra-Tschuschke, I., et al. (2019). A polyextreme hydrothermal system controlled by iron: the case of Dallol at the Afar Triangle. *ACS Earth Space Chem.* 3, 90–99. doi: 10.1021/acsearthspacechem.8b00141
- Lalou, C., Van Nguyen, H., Faure, H., and Moreira, L. (1970). Datation par la méthode uranium-thorium des hauts niveaux de coraux de la dépression de l’Afar (Ethiopie). *Rev. Géogr. Phys. Géol. Dyn.* 12, 3–8.
- MacDonald, G. J. F. (1953). Anhydrite gypsum equilibrium relations. *Am. J. Sci.* 251, 884–898. doi: 10.2475/ajs.251.12.884
- Mitchell, D. J. W., Allen, R. B., Salama, W., and Abouzakm, A. (1992). Tectonostratigraphic framework and hydrocarbon potential of the Red Sea. *J. Pet. Geol.* 15, 187–210. doi: 10.1111/j.1747-5457.1992.tb00962.x
- Nobile, A., Pagli, C., Keir, D., Wright, T. J., Ayele, A., Ruch, J., et al. (2012). Dike-fault interaction during the 2004 Dallol intrusion at the northern edge of the Erta Ale Ridge (Afar, Ethiopia). *Geophys. Res. Lett.* 39, 2–7. doi: 10.1029/2012GL053152
- Omosanya, K. O., Eruteya, O. E., Siregar, E. S. A., Zieba, K. J., Johansen, S. E., Alves, T. M., et al. (2018). Three-dimensional (3-D) seismic imaging of conduits and radial faults associated with hydrothermal vent complexes (Vøring Basin, Offshore Norway). *Mar. Geol.* 399, 115–134. doi: 10.1016/j.margeo.2018.02.007
- Pagli, C., Wright, T. J., Ebinger, C. J., Yun, S.-H., Cann, J. R., Barnie, T., et al. (2012). Shallow axial magma chamber at the slow-spreading Erta Ale Ridge. *Nat. Geosci.* 5, 284–288. doi: 10.1038/ngeo1414
- Pedgley, D. E. (1967). Air temperature at Dallol, Ethiopia. *Meteorol. Mag.* 96, 265–270. doi: 10.1175/1520-0493192048<219e:tmm<2.0.co;2
- Planke, S., Rasmussen, T., Rey, S. S., and Myklebust, R. (2005). Seismic characteristics and distribution of volcanic intrusions and hydrothermal vent complexes in the Vøring and More basins. *Geol. Soc. Lond., Pet. Geol. Conf. Ser.* 6, 833–844. doi: 10.1144/0060833
- Reilinger, R., and McCluskey, S. (2011). Nubia-Arabia-Eurasia plate motions and the dynamics of Mediterranean and Middle East tectonics. *Geophys. J. Int.* 186, 971–979. doi: 10.1111/j.1365-246X.2011.05133.x

- Tadiwos, C. (2013). "Dallol volcano and Danakil depression?: earth resources and geo-hazards," in *Proceedings of the 24th Colloquium of African Geology and 14th Congress of Geological Society of Africa, Aveiro*.
- Talbot, C. J. (2008). Hydrothermal salt-but how much? *Mar. Pet. Geol.* 25, 191–202. doi: 10.1016/j.marpetgeo.2007.05.005
- Tesfaye, S., Harding, D. J., and Kusky, T. M. (2003). Early continental breakup boundary and migration of the Afar triple junction, Ethiopia. *GSA Bull.* 115, 1053–1067.
- Varet, J. (2010). "Contribution to favorable geothermal site selection in the Afar triangle," in *Proceedings of the ARGEO-C3 Third East African Rift Geothermal Conference, Djibouti*, 139–155.
- Varet, J. (2018). "Recent and active units of the Danakil Sea (Dagad Salt Plain) and Afdera Lake," in *Geology of Afar (East Africa)* (Cham: Springer International Publishing), 205–226. doi: 10.1007/978-3-319-60865-5_7
- Warren, J. K. (2015a). *Danakhil Potash, Ethiopia: Beds of Kainite/Carnallite, Part 2 of 4*. Technical Report. Adelaide, SA: SaltWork Consultants Pte Ltd. doi: 10.13140/RG.2.1.2392.9769
- Warren, J. K. (2015b). *Danakhil Potash, Ethiopia: Is the Present Geology the Key? Part 1 of 4*. Technical Report. Adelaide, SA: SaltWork Consultants Pte Ltd. doi: 10.13140/RG.2.1.4752.2728
- Warren, J. K. (2015c). *Danakhil Potash; Ethiopia – Modern Hydrothermal and Deep Meteoric KCl, Part 3 of 4*. Technical Report. Adelaide, SA: SaltWork Consultants Pte Ltd. doi: 10.13140/RG.2.1.4883.3443
- Warren, J. K. (2015d). *Danakil Potash: K₂SO₄ Across the Neogene: Implications for Danakhil Potash, Part 4 of 4*. Technical Report. Adelaide, SA: SaltWork Consultants Pte Ltd. doi: 10.13140/RG.2.1.2098.0648
- Wunderman, R. (ed.) (2013). "Report on Dallol (Ethiopia)," in *Bulletin of the Global Volcanism Network*, Vol. 38, ed. R. Wunderman, (Washington, DC: Smithsonian Institution). doi: 10.5479/si.GVP.BGVN201305-221041
- Zeyen, N., Benzerara, K., Li, J., Groleau, A., Balan, E., Robert, J. L., et al. (2015). Formation of low-T hydrated silicates in modern microbialites from Mexico and implications for microbial fossilization. *Front. Earth Sci.* 3:64. doi: 10.3389/feart.2015.00064

Conflict of Interest: The authors declare that the research was conducted in the absence of any commercial or financial relationships that could be construed as a potential conflict of interest.

Copyright © 2020 López-García, Moreira, Benzerara, Grunewald and López-García. This is an open-access article distributed under the terms of the Creative Commons Attribution License (CC BY). The use, distribution or reproduction in other forums is permitted, provided the original author(s) and the copyright owner(s) are credited and that the original publication in this journal is cited, in accordance with accepted academic practice. No use, distribution or reproduction is permitted which does not comply with these terms.